Accepted Manuscript

Timescales of magma ascent and degassing and the role of crustal assimilation at Merapi volcano (2006-2010), Indonesia: constraints from uranium-series and radiogenic isotopic compositions

H.K. Handley, M. Reagan, R. Gertisser, K. Preece, K. Berlo, L.E. McGee, J. Barclay, R. Herd

Please cite this article as: Handley, H.K., Reagan, M., Gertisser, R., Preece, K., Berlo, K., McGee, L.E., Barclay, J., Herd, R., Timescales of magma ascent and degassing and the role of crustal assimilation at Merapi volcano (2006-2010), Indonesia: constraints from uranium-series and radiogenic isotopic compositions, *Geochimica et Cosmochimica Acta* (2017), doi: https://doi.org/10.1016/j.gca.2017.10.015
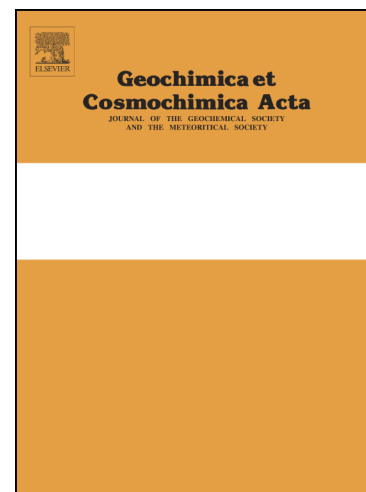
1   For submission to Geochimica et Cosmochima Acta

2

3

4   Timescales of magma ascent and degassing and the role of crustal assimilation

5   at Merapi volcano (2006-2010), Indonesia: constraints from uranium-series and

6   radiogenic isotopic compositions

7

8

9

10   H. K. Handley[1*], M. Reagan[2], R. Gertisser[3], K. Preece[4,5], K. Berlo[6], L. E. McGee[1], J.

11   Barclay[4], R. Herd[4]

12

13   [1]Department of Earth and Planetary Sciences, Macquarie University, Sydney, NSW 2109,

14   Australia

15   [2] Department of Earth and Environmental Sciences, The University of Iowa, Iowa City, IA

16   52242, USA

17   [3]School of Geography, Geology and the Environment, Keele University, Keele, ST5 5BG,

18   UK

19   [4]School of Environmental Sciences, University of East Anglia, Norwich, NR4 7TJ, UK

20   [5]Isotope Geoscience Unit, Scottish Universities Environmental Research Centre, East

21   Kilbride, G75 0QF, UK

22   [6]Department of Earth and Planetary Sciences, McGill University, Montreal, H3A 0E8,

23   Canada

24

25

26

27

30

31   *Corresponding author. Department of Earth and Planetary Sciences, Macquarie University,

32   Sydney, NSW 2109 Australia. Telephone: +61 2 9850 4403. Fax: +61 2 9850 8943. Email:

33   heather.handley@mq.edu.au

Abstract

We present new ^{238}U-^{230}Th-^{226}Ra-^{210}Pb-^{210}Po, ^{87}Sr/^{86}Sr and ^{143}Nd/^{144}Nd isotopic data of whole-rock samples and plagioclase separates from volcanic deposits of the 2006 and 2010 eruptions at Merapi volcano, Java, Indonesia. These data are combined with available eruption monitoring, petrographic, mineralogical and Pb isotopic data to assess current theories on the cause of a recent transition from effusive dome-building (2006) to explosive (2010) activity at the volcano, as well as to further investigate the petrogenetic components involved in magma genesis and evolution. Despite the significant difference in eruption style, the 2006 and 2010 volcanic rocks show no significant difference in (^{238}U/^{232}Th), (^{230}Th/^{232}Th) and (^{226}Ra/^{230}Th) activity ratios, with all samples displaying U and Ra excesses. The ^{226}Ra and ^{210}Pb excesses observed in plagioclase separates from the 2006 and 2010 eruptions indicate that a proportion of the plagioclase grew within the decades preceding eruption. The 2006 and 2010 samples were depleted in ^{210}Po relative to ^{210}Pb ((^{210}Po/^{210}Pb)$_i$ <1) at the time of eruption but were variably degassed (69% to 100%), with the degree of ^{210}Pb degassing strongly related to sample texture and eruption phase. In good agreement with several activity monitoring parameters, ^{210}Po ingrowth calculations suggest that initial intrusion into the shallow magma plumbing system occurred several weeks to a few months prior to the initial 2010 eruption. The 2006 and 2010 samples show a wide range in (^{210}Pb/^{226}Ra) activity ratio within a single eruption at Merapi and are largely characterised by ^{210}Pb deficits ((^{210}Pb/^{226}Ra) <1). Assuming a model of complete radon degassing, the ^{210}Pb deficits in the 2006 volcanic rocks indicate relatively longer degassing timescales of ~2-4 years than those given by the 2010 samples of ~0-3 years. The uranium-series and radiogenic isotopic data do not support greater crustal assimilation of carbonate material as the explanation for the more explosive behaviour of Merapi in 2010 (as has been previously suggested) and instead indicate that relatively rapid ascent of a more undegassed magma was the primary difference responsible for the transition in explosive behaviour. This interpretation is in good agreement with gas monitoring data, previous petrological studies (mineral, microlite and melt inclusion work) and maximum calculated timescale estimates using Fe-Mg compositional gradients in clinopyroxene, that also suggest more rapid movement of relatively undegassed magma in 2010 relative to 2006.

1. Introduction

Many volcanoes undergo relatively rapid changes in eruption explosivity, often exhibiting transitions between effusive and explosive behaviour both within and between eruptions,

2

68   such as at Soufriere Hills Volcano, Lesser Antilles (e.g., Edmonds and Herd, 2007),

69   Novarupta, Alaska (e.g., Nguyen et al., 2014) Kelut, Indonesia (e.g., Jeffery et al., 2013) and

70   Volcán de Colima, Mexico (e.g., Zobin et al., 2015). Therefore understanding the drivers of

71   such change is of great importance for volcanic hazard mitigation.

72   Merapi Volcano, located 25 km north of Yogyakarta in Central Java in the Sunda arc,

73   is one of the most active volcanoes in Indonesia. The 2010 explosive eruption was the

74   volcano's largest eruption since 1872, resulted in the highest number of fatalities since the

75   1930 eruption and was much more violent than expected. Prior to the 2010 eruption, recent

76   volcanic activity at Merapi was characterised by the growth and collapse of lava domes (e.g.,

77   Andreastuti et al., 2000; Camus et al., 2000; Newhall et al., 2000; Voight et al., 2000;

78   Gertisser et al., 2012), for example, as witnessed in 2006 (Charbonnier and Gertisser, 2008;

79   2011; Preece et al., 2013; Ratdomopurbo et al., 2013). Whether eruptions at Merapi are

80   effusive or explosive in character is thought to result from a number of factors, such as

81   variations in magma supply from depth, magma ascent rate, magma degassing behaviour and

82   the assimilation of crustal carbonates (Newhall et al., 2000; Gertisser and Keller, 2003a;

83   Chadwick et al., 2007; Deegan et al. 2010; Surono et al., 2012; Troll et al., 2012; 2013;

84   Borisova et al., 2013; 2016; Costa et al., 2013; Preece et al., 2013; 2014; 2016). Petrologic

85   and monitoring data suggest the rapid ascent of a significantly larger, volatile-rich (i.e.

86   relatively undegassed) magma body, and its possible interaction with crustal carbonates,

87   caused the significant change in explosive behaviour of the volcano between 2006 and 2010

88   (Surono et al., 2012; Borisova et al., 2013; Costa et al., 2013; Preece et al., 2013; 2014; 2016;

89   Erdmann et al., 2016).

90   The uranium-series (U-series) nuclides provide unique timescale information on

91   magmatic processes ranging from melt production, differentiation and ascent to magmatic

92   degassing prior to eruption (e.g., Bennett et al., 1982; Gill and Williams, 1990; Turner et al.,

93   2000; Condomines et al., 2003; Peate and Hawkesworth 2005; Bourdon et al., 2006; Reagan

94   et al., 2006; Handley et al., 2008; Reagan et al., 2008; Berlo et al., 2010; Sims et al., 2013;

95   Bragagni et al., 2014) as the nuclides have varied geochemical properties that cause them to

96   be fractionated in distinct ways by different magmatic processes (see Peate and Hawkesworth

97   (2005) for a review). At secular equilibrium the activities of the nuclides (denoted by

98   parentheses) are equal, for example, $(^{230}Th/^{238}U) = 1$. If the decay chain is affected by

99   chemical fractionation of a parent/daughter elemental ratio, restoration of equilibrium by

100   radioactive decay is determined by the half-life of the daughter nuclide involved. Excess ^{238}U

101   $((^{238}U/^{230}Th)>1)$ and ^{226}Ra $((^{226}Ra/^{230}Th) >1)$ in subduction zone volcanic rocks are typically

102   attributed to fluid addition from the subduction slab on timescales of less than ~380,000 years

103   and less than ~8,000 years, respectively (e.g., Condomines et al., 1988; Gill and Williams,

104   1990; Hawkesworth et al., 1997) although there may be some modification of ratios by

105   crustal-level processes (e.g., Handley et al., 2008; Reubi et al., 2014; Huang et al., 2016). At

106   magmatic temperatures, ^{234}U is not expected to be fractionated from ^{238}U, and so fresh

107   igneous rocks should have $(^{234}U/^{238}U) = 1$.

108   Detailed studies of the shorter-lived U-series nuclides from individual volcanic

109   centres, for example, ^{210}Po (half-life = 138.4 days) and its 'grandparent' ^{210}Pb (half-life =

110   22.6 years), require the collection of young, fresh and dated samples that need to be analysed

111   within a short timeframe after eruption. Polonium partitions efficiently into exsolving volatile

112   phases and is almost completely lost during eruption (Bennett et al., 1982; Gill et al., 1985,

113   Rubin and Macdougall, 1989; Reagan et al., 2008), which results in $(^{210}Po/^{210}Pb) \ll 1.0$ in

114   erupted lavas. The short-lived ^{210}Pb nuclide is produced by decay of the gas ^{222}Rn (half-life =

115   3.8 days), which readily enters the volatile phase in magmas (Lambert et al., 1985; Gill et al.,

116   1985). Persistent loss or gain of ^{222}Rn via magmatic degassing or volatile accumulation will

117   therefore create disequilibrium between the nuclides situated before and after ^{222}Rn, that is

118   between the parent ^{226}Ra and the daughter ^{210}Pb. As a result, in an open, degassing system

119   where ^{222}Rn is efficiently lost in the gas phase, deficits of ^{210}Pb are expected, i.e.

120    $(^{210}Pb/^{226}Ra) < 1$. Thus, ^{210}Pb deficits can constrain the duration of degassing (e.g., Gauthier

121   and Condomines, 1999). Alternatively, if gas is supplied from underlying fresh (and probably

122   more mafic) magma, it is possible to create a ^{210}Pb excess (e.g., Kayzar et al., 2009;

123   Condomines et al., 2010).

124   Previous ^{210}Pb-^{226}Ra disequilibria measurements on Merapi volcanic rocks erupted

125   between 1981-1995 showed variable initial $(^{210}Pb/^{226}Ra)$ ratios, from 0.75 to 1 (Gauthier and

126   Condomines, 1999). Based on these data, a <10-year cycle of closed-system magmatic

127   evolution with open degassing followed by episodes of undegassed magmatic recharge was

128   proposed for Merapi (Gauthier and Condomines, 1999). In a study of (^{210}Pb), (^{210}Bi), and

129   (^{210}Po) activities and SO_2 in Merapi gaseous emissions conducted between 1978–1995, it was

130   found that growing dome magma had been completely degassed when it reached the surface.

131   It was also suggested that the non-explosive (dome-building) eruptions arise due to open-

132   system degassing at depth beneath the volcano (Le Cloarec and Gauthier, 2003).

133   Abundant, young volcanic samples from progressive phases of the dome-forming

134   eruption in 2006 and the highly explosive eruption in 2010 at Merapi volcano, provide a rare

135   opportunity to conduct a detailed ^{210}Po-^{210}Pb-^{226}Ra disequilibria study and provide insight

from ^{238}U-^{230}Th-^{226}Ra-^{210}Pb-^{210}Po disequilibria and Sr-Nd-Pb isotopic compositions on magmatic source components, the role of assimilation of carbonate material and the timescales of magmatic degassing. The data are used to assess current theories on the recent transition from effusive to explosive eruption at Merapi (e.g., Surono et al., 2012; Borisova et al., 2013; 2016; Costa et al., 2013; Preece et al., 2013; 2014; 2016; Erdmann et al., 2016) and to further investigate the proposed periodicity in magmatic degassing and recharge at Merapi (Gauthier and Condomines, 1999) over a longer time period, ending with the cataclysmic eruption in 2010.

2. Summary of the 2006 and 2010 volcanic eruptions of Merapi

Over the last two centuries, dominant volcanic activity at Merapi has characteristically consisted of the growth and collapse of basaltic-andesite lava domes, producing relatively small-volume pyroclastic density currents (PDCs) on a periodicity of 4-6 years, with larger explosive eruptions recurring on the order of centuries (Andreastuti et al., 2000; Camus et al., 2000; Newhall et al, 2000; Voight et al., 2000; Gertisser et al., 2012).

The April to October 2006 eruption (Volcanic Explosivity Index (VEI) 1) was characterised by typical recent Merapi activity, with episodes of lava dome growth and collapse. Early eruption seismic precursors suggest that the first signs of new activity were detected by seismic and deformation data in July 2005, which increased from December 2005 to mid-April 2006 (Ratdomopurbo et al., 2013). The full chronology of events of the 2006 eruption can be found in Charbonnier and Gertisser (2008; 2011), Preece et al. (2013) and Ratdomopurbo et al. (2013). Lava dome extrusion likely began between 26-28 April 2006 and continued throughout May, with the first dome collapses on 11 May, producing PDCs extending less than 4 km from the summit to the southwest. Three major collapse stages took place from 4 to 14 June (Charbonnier and Gertisser, 2008, 2011; Ratdomopurbo et al., 2013) destroying most of the dome and forming a series of PDCs that reached up to 7 km from the summit at the peak of activity on 14 June (Charbonnier and Gertisser, 2008, 2011; Lube et al., 2011; Ratdomopurbo et al., 2013). A new lava dome was observed inside the new crater on 26 June, which continued to grow until October 2006 (Preece et al., 2013; Ratdomopurbo et al., 2013).

In contrast, the following October-November 2010 eruption (VEI 4) at Merapi was the largest eruption since 1872 (Surono et al., 2012). After approximately one year of unrest and intrusion (Stage 1; 31 October 2009 to 25 October 2010), initial phreatomagmatic explosions occurred between 26 and 29 October (Stage 2) (Komorowski et al., 2013),

170 followed by recurrent rapid dome growth and destruction during 29 October to 4 November

171 (Stage 3). Dome extrusion rates in 2010 were extremely rapid at >25 m^3s^{-1} on average

172 (Pallister et al., 2013) compared to 1 to 4 $m^3 s^{-1}$ for the 2006 eruption (Ratdomopurbo et al.,

173 2013). A series of laterally-directed explosions (Stage 4) and retrogressive dome collapses

174 (Stage 5) occurred during the climactic eruption phase on 5 November. These produced

175 valley-confined, concentrated pyroclastic density currents that travelled up to ~16 km from

176 the summit, and contemporaneous widespread, high-energy pyroclastic density currents.

177 Sulphur dioxide emission levels also peaked at this time (Surono et al., 2012; Fig. 1).

178 Following a sub-Plinain phase and fountain collapse (Stage 6), further dome growth and

179 multiple ash plumes continued until 8 November (Stage 7). The activity waned towards the

180 end of November (Stage 8), with decreasing intensity of gas and ash emissions (e.g., Surono

181 et al., 2012; Charbonnier et al., 2013; Cronin et al., 2013; Komorowski et al., 2013; Preece et

182 al., 2014; 2016). Detailed chronological accounts of the eruption (noting slight discrepancies

183 in eruption timings between accounts) are presented in Surono et al. (2012), Charbonnier et

184 al. (2013), Cronin et al. (2013), Komorowski et al. (2013) and Preece et al. (2014). The

185 estimated deposit (non-DRE) volume for the 2010 eruption of ~ 30-60 x 10^6 m^3 (Surono et

186 al., 2012; Charbonnier et al., 2013) is also much greater than that for the 2006 eruption at

187 ~8.7 x 10^6 m^3 (Charbonnier and Gertisser, 2011). In the months preceding the 2010 eruption,

188 a significant increase in CO_2 abundance (10 wt% to 35-63 wt% from September to 20

189 October) and CO_2/SO_2, CO_2/HCl and CO_2/H_2O ratios suggested a progressive shift to a deep

190 degassing source (Surono et al., 2012), which has been corroborated by petrological studies

191 (Costa et al., 2013; Preece et al., 2014; 2016). Time-series of SO_2 flux estimated from

192 ground-DOAS and satellite measurements show that the SO_2 emission rates during the 2010

193 eruption were orders of magnitude higher than during the previous eruption period in 2006

194 (Fig. 1) and were correlated with energetic tremor and high eruption rates during the most

195 explosive phases of the eruption (Surono et al., 2012). High SO_2 emissions accompanied the

196 initial explosive eruptions on 26 October and again between 29-30 October 2010. The

197 emissions then decreased during the extrusion and growth of a lava dome and peaked during

198 the climatic phase of the eruption on 5 November (Surono et al., 2012) (Fig. 1).

199 Juvenile material erupted in both 2006 and 2010 displays similar whole-rock

200 compositions of ~55-56 wt% SiO_2 (Surono et al., 2012; Costa et al., 2013; Preece et al.,

201 2013; 2014; 2016) and similar mineral assemblages dominated by plagioclase with

202 clinopyroxene, orthopyroxene and minor amphibole and titanomagnetite. However, most

203 amphibole phenocrysts in the juvenile 2010 material do not show reaction rims, whereas

204 many within the 2006 deposits are largely reacted (Surono et al., 2012; Costa et al., 2013;

205 Preece at al., 2013, 2014). The lack of amphibole reaction rims in 2010 deposits along with

206 microlite textural and compositional analysis, suggest minimal storage and relatively rapid

207 movement of the 2010 magma relative to that erupted in 2006 (Preece et al., 2013; 2014;

208 2016).

209

210 **3. Samples and analytical procedures**

211 A summary of the sample textural types selected for U-series isotopic analysis is given in

212 Tables 1 and 2. A detailed description of samples (except MER061406-L and MER061406-

213 D) can be found in Preece (2014) and Preece et al. (2013; 2014; 2016). Samples

214 MER061406-L and MER061406-D are scoriaceous fragments collected from a PDC deposit

215 erupted 14 June, 2006. The "L" sample is light grey, highly crystalline and has ~30%

216 vesicles. The sample contains about 30% plagioclase (<1.3 mm in length), 5% clinopyroxene

217 (<0.7 mm), 3% magnetite (<0.2 mm), and < 1% hornblende (<1 mm) and orthopyroxene

218 (<0.3 mm). Plagioclase is euhedral, complexly zoned and typically has abundant inclusions

219 of glass, magnetite, and clinopyroxene. Clinopyroxene also is euhedral with abundant

220 inclusions of magnetite and apatite. Hornblende is anhedral with variably thick reaction rims

221 of plagioclase, orthopyroxene, magnetite, and clinopyroxene. Orthopyroxene is anhedral with

222 optically continuous clinopyroxene rims. The remaining approximately 30% is groundmass

223 consisting of glass, plagioclase, magnetite, orthopyroxene, and clinopyroxene. The "D" (dark

224 grey-brown) sample is similarly vesicular and highly crystalline, but has a more mafic

225 mineral assemblage of ~40% complexly zoned plagioclase (< 1 mm), 10% clinopyroxene (<

226 1mm), 3% magnetite (<0.1 mm), and < 1% olivine (<1 mm). The olivine is anhedral with

227 ~0.1 mm reaction rims of granular clinopyroxene. The groundmass in this sample is finely

228 holocrystalline, mostly plagioclase and partially oxidized magnetite.

229 The relationship of samples to the eruption chronology is given in Table 1 and

230 follows that presented in Preece et al. (2013) for the 2006 eruption, and Komorowski et al.

231 (2013) and Preece et al. (2014; 2016) for the 2010 eruption. The light grey dense inclusions

232 (LGD-Inc) are found as abundant angular inclusions ranging from millimetres to centimetres

233 in size within the juvenile dome material. Occasionally, this lithology forms diffuse bands

234 through the darker dome material and large, sometimes prismatically-jointed blocks (up to

235 several metres in diameter) of this material have been found loose within the 2010 Stage 4

236 PDC deposits (Preece et al., 2016). There is some degree of uncertainty in the exact extrusion

237 age of juvenile dense clasts from pyroclastic density current deposits, as for example, for the

238   2010 eruption, the juvenile dome material that collapsed on the 5 November was extruded

239   anytime between 29 October and 4 November (see Table 1 footnote for further details on

240   assumed eruptive age). However for the (^{210}Po) activities (which would be most affected by

241   assumptions in extrusion age), whether the 29 October or 4 November is selected as the

242   extrusion age, the calculated initial (^{210}Po) activities lie within 2σ error of each other.

243   Fresh samples MER061406-L and MER061406-D were ultrasonically washed in

244   purified water, dried, reduced in a jaw crusher, and ground to powder in a ceramic mill. All

245   other samples had any weathered edges removed prior to washing in deionized water, drying

246   and processing to powder in an agate mill (Preece et al., 2013; Preece 2014). U, Th and Ra

247   concentrations and isotopic ratios were determined on bulk-rock powders and plagioclase

248   separates using the procedure employed by the Uranium-series Research Laboratory at

249   Macquarie University GeoAnalytical (MQGA) for volcanic rock samples. Approximately 0.5

250   g of bulk-rock powder or 2 g of plagioclase separate was spiked with ^{236}U-^{229}Th and ^{228}Ra

251   tracers and digested in a mixture of concentrated acids (HF-HNO$_3$-HCl). Separation of U and

252   Th followed standard anionic resin chromatography as described in Turner et al. (2011).

253   Uranium and thorium concentrations, determined by isotope dilution, and U-Th isotopic

254   ratios were measured on a Nu Instrument Multi-Collector inductively coupled plasma mass

255   spectrometer (MC-ICP-MS) at Macquarie University following the approach given by Turner

256   et al. (2011). In addition, the New Brunswick Laboratory (NBL) U010 synthetic standard was

257   used to carry out linear drift correction and normalisation of samples for U isotopes, using the

258   certified atomic ratios of 5.47 x 10^{-5}, 1.01 x 10^{-2} and 6.88 x 10^{-5} for ^{234}U/^{238}U, ^{235}U/^{238}U and

259   ^{236}U/^{238}U, respectively. The NBL synthetic standard U005-A was run as an unknown at

260   regular intervals throughout the analytical session to assess the robustness of instrumental

261   corrections. The average corrected U005-A ^{234}U/^{238}U, ^{235}U/^{238}U and ^{236}U/^{238}U ratios (n = 8)

262   were 3.42 ± 0.01 x 10^{-5} (2SD), 5.09 ± 0.01 x 10^{-3} (2SD) and 1.18 ± 0.01 x 10^{-5} (2SD), which

263   are within error of the NBL published values of 3.42 x 10^{-5}, 5.09 x 10^{-3} and 1.19 x 10^{-5}.

264   Similarly, the UCSC Th 'A' was used as a monitor of the robustness of instrumental

265   corrections during the analytical session. The average corrected Th 'A' (using the Th 'U'

266   bracketing method detailed in Turner et al., 2011) ^{230}Th/^{232}Th ratio was 5.83 x 10^{-6} ± 0.04 x

267   10^{-6} (2SD, n = 7), which is within error of the recommended ratio of 5.86 x 10^{-6} given by

268   Sims et al. (2008) taken from Rubin (2001). The Table Mountain Latite (TML) rock standard,

269   was digested and fully processed alongside the samples in each batch (n = 2) and the data are

270   presented in Table 1. The (^{238}U/^{232}Th), (^{230}Th/^{232}Th) analyses of TML lie within error of

271 published values (e.g. Sims et al., 2008; Sims et al., 2013). However, the $(^{230}Th/^{238}U)$

272 deviates by 2.5% from equilibrium. It is possible that due to the corrections required for MC-

273 ICP-MS data (e.g., instrumental fractionation, ^{232}Th-tailing corrections and the uncertainties

274 on half-lives) compared to measurements by alpha-spectrometry, that ^{230}Th is slightly

275 underestimated for our samples. Nevertheless, there is no significant difference in U-Th

276 isotopic ratios of the 2006 and 2010 rocks (Fig. 2). Replicate analysis of M11-05 and M07-

277 53P gave $(^{234}U/^{238}U)$, $(^{238}U/^{232}Th)$, $(^{230}Th/^{232}Th)$ and $(^{238}U/^{230}Th)$ activity ratios within error

278 of the initial analyses (Table 1). The Ra separation and analysis procedure follows that

279 described by Turner et al. (2000; 2011). Samples were loaded onto degassed single Re

280 filaments using a Ta-HF-H$_3$PO$_4$ activator solution (Birck, 1986) and $^{228}Ra/^{226}Ra$ ratios were

281 measured in dynamic ion counting mode on a ThermoFinnigan Triton TIMS at Macquarie

282 University. Accuracy was assessed via analysis of TML that yielded ^{226}Ra = 3594 fg/g and

283 $(^{226}Ra/^{230}Th)$ = 1.005 ± 0.008 (2SE), within internal analytical error of secular equilibrium.

284 The Merapi $(^{230}Th/^{232}Th)$ and $(^{226}Ra/^{230}Th)$ ratios have not been recalculated for differences

285 in eruption age as samples were analysed within 10 years of eruption and therefore, post-

286 eruption radioactive decay is insignificant compared to the half-life of ^{230}Th (75,690 years)

287 and ^{226}Ra (1599 years).

288   Analyses of ^{210}Po by alpha counting were performed at the University of Iowa, using

289 methods described by Reagan et al. (2005; 2006) and Waters et al. (2013). Approximately 2

290 grams of whole rock powder or 3 grams of separated plagioclase were used for each ^{210}Po

291 analysis. All whole rock powders with ages of less than two years and the plagioclase mineral

292 separate were leached for 5 minutes in cold 0.5 N HCl using an ultrasonic agitator and triply

293 washed in purified water. Older samples were ultrasonically washed in purified water.

294 Samples and some supernates were spiked with a ^{209}Po solution calibrated against the TML

295 standard and monitored with repeat analysis of RGM-2. The samples were subsequently

296 digested using an HF-HNO$_3$ method, dried, dissolved in 1N HCl, and the solution passed

297 through anion exchange resin to separate Po. Polonium was washed off the resin in warm 7.5

298 N HNO$_3$. The separated Po was autoplated on Ag in 0.5 N HCl and counted using an EGG

299 Ortec alpha spectrometer. The 1995 sample and most 2006 samples were more than two

300 years old at the time of measurement, i.e. five times the half-life of ^{210}Po (138.4 days) and

301 therefore, (^{210}Pb) was considered equal to (^{210}Po). For the 2006 and 2010 samples repeatedly

302 analysed soon (< 2 years) after eruption, the initial ^{210}Pb activities, $(^{210}Pb)_i$, representing ^{210}Pb

303 activity at the time of eruption, and associated uncertainties were obtained through a Markov

9

304　Chain Monte Carlo simulation using Matlab. Only best-fitting models that fitted the data
305　within analytical uncertainties were considered in the computation.

306　　　　Samples for Sr and Nd isotopic analysis (from the same sample digestion as for U-Th
307　isotopes) were prepared and analysed at the MQGA at Macquarie University. Sr and REE
308　fractions were separated using a cationic column containing Biorad® AG50W-X8 (200-400
309　mesh) cationic exchange resin, after which Sm and Nd were separated using EIChrom® LN-
310　spec resin following the column procedure given by Pin et al. (1997). Samples were loaded on
311　to out-gassed single (Sr) and double (Nd) rhenium filaments using 2 μl of $TaCl_5$ + HF +
312　H_3PO_4 + H_2O_2 and 5 μl of 1N HCl: 0.35N H_3PO_4 activator solutions, respectively. Analyses
313　were performed in static mode on a ThermoFinnigan Triton® TIMS in the MQGA.
314　Instrument mass fractionation was accounted for by normalizing $^{87}Sr/^{86}Sr$ and $^{143}Nd/^{144}Nd$ to
315　$^{87}Sr/^{86}Sr$ = 0.1194 and $^{143}Nd/^{144}Nd$ = 0.7219, respectively. Sr and Nd blanks were lower than
316　1000 and 80 pg, respectively. Analysis of NIST SRM-987 gave 0.710214 ± 8 (2SE) and the
317　JMC Nd standard gave 0.511116 ± 8 (2SE).

318

319　**4. Results**

320　*4.1. ^{238}U-^{230}Th-^{226}Ra disequilibria in whole-rock samples and plagioclase*

321　The new 2006 and 2010 Merapi whole-rock samples and plagioclase separates have U
322　excesses (($^{238}U/^{230}Th$) activity ratios > 1) (Table 1, Fig. 2a), typical of subduction-related
323　volcanic rocks. The 2010 samples show slightly greater variation in ($^{238}U/^{232}Th$) and
324　($^{230}Th/^{232}Th$) compared to the 2006 samples, although the data for both eruptions largely
325　overlap. The new data in this study overlap with but display slightly lower ($^{230}Th/^{232}Th$)
326　compared to the previously published, whole-rock Merapi data (Fig. 2a), which were largely
327　produced by alpha spectrometry.

328　　　　The 2006 and 2010 Merapi whole-rock samples and plagioclase separates have excess
329　radium (($^{226}Ra/^{230}Th$) > 1) (Table 1, Fig. 2b) with no significant difference between the 2006
330　and 2010 whole-rock samples, and the majority of ($^{226}Ra/^{230}Th$) ratios lying between 3.0-3.3.
331　The plagioclase separates also show similar ($^{226}Ra/^{230}Th$) ratios between the two eruptions of
332　3.5-3.7. The previously published historical and recent, whole-rock Merapi data (Gill and
333　Williams, 1990; Gauthier and Condomines, 1999; Condomines et al., 2005) show comparable
334　excess Ra values to the 2006 and 2010 samples (Fig. 2b).

335

336　*4.2 ^{210}Po- ^{210}Pb-^{226}Ra disequilibria*

10

337   Repeated analysis of (^{210}Po) in leached, whole-rock material of two 2006 samples and the

338   2010 samples, all collected shortly after eruption, was carried out to constrain the initial ^{210}Po

339   activity at the time of eruption (Table 2), i.e. where the growth curve intersects the y-axis at

340   zero days since eruption in Fig. 3. The repeated sample measurements lie within analytical

341   error of a single growth curve apart from sample MER061406-D, which has a high initial

342   ^{210}Po activity of 2.95 dpm/g (Table 2; Fig. 3) and is therefore, not a juvenile fragment of the

343   2006 eruption. Excluding MER061406-D, the results show that the 2006 and 2010 samples

344   were all depleted in ^{210}Po relative to ^{210}Pb ((^{210}Po/^{210}Pb)$_i$ < 1) at the time of eruption but were

345   variably degassed (Table 2). The 2006 sample, MER061406-L, was 93% degassed on

346   eruption with an initial (^{210}Po) of 0.21 (Table 2). For the 2010 samples, the pre-Nov 5 scoria

347   (S2S; M11-28a) and light grey dense inclusion (LGD-Inc; M11-28b) samples erupted at the

348   beginning of the eruptive period (26 October, Stage 2 of Komorowski et al., 2013), display

349   intermediate initial (^{210}Po) compared to the other 2010 samples. The scoria sample has a

350   lower initial (^{210}Po) compared to the LGD-Inc sample and is also relatively more degassed on

351   eruption (87% compared to 74%). The dark dense, lava dome (DD) samples (M11-27-5 and

352   M11-12) extruded during stage 3, i.e., the dome extrusion phase between 29 October and 4

353   November (Komorowski et al., 2013; Table 2) and emplaced in PDCs during stage 4

354   (labelled 1 Nov in Fig. 3) show the lowest initial (^{210}Po) and are 97% to 100% degassed of

355   ^{210}Po at the time of eruption, which contrasts to the light grey inclusion (LGD-Inc; M11-05)

356   from the same stage (Table 2). The LGD-Inc shows the highest initial (^{210}Po) and was 69%

357   degassed of ^{210}Po at the time of eruption ((^{210}Po/^{210}Pb)$_i$ = 0.31, Table 2). The white pumice

358   (WP; M11-18) erupted during sub-plinian fountaining on 5 November (Stage 6 of

359   Komorowski et al., 2013) was 83% degassed of ^{210}Po at the time of eruption (Table 2).

360   The majority of the 2006 Merapi volcanic rocks were analysed several years post-

361   eruption and therefore, due to the short half-life of ^{210}Po (138.4 days), the measured (^{210}Po)

362   equates to the initial (^{210}Pb) at measurement date for these samples. The range in initial

363   (^{210}Pb) activities for the 2006 samples analysed more than 2 years post-eruption (2.57-3.15

364   dpm/g, Table 2), are shown plotted along the right-hand y-axis in Fig. 3 and lie within the

365   range displayed by the 2010 samples and sample MER061406-L from 2006 (comparing with

366   the (^{210}Po) activities from the growth curves at ~800 days). The initial (^{210}Pb) activities

367   determined from best-fit growth curves are relatively similar for the samples erupted in the

368   middle stage of the 2010 eruption (2.93-3.13 dpm/g) but higher than those determined for the

369   samples erupted earlier, on 26 October, in Stage 2 (2.38-2.64 dpm/g) (Table 2).

11

370   The initial $(^{210}Pb/^{226}Ra)_0$ activity ratios, calculated to the time of eruption, of the 2006

371   and 2010 Merapi volcanic rocks are presented in Table 2 and Fig. 1. The variation observed

372   in $(^{210}Pb/^{226}Ra)_0$ for each of the 2006 and 2010 eruptions is comparable to the full range of

373   ratios measured in the time period from 1981 to 1995, previously reported by Gauthier and

374   Condomines (1999). With the exception of one DD 2010 sample (M11-27-5), the 2006 and

375   2010 samples are largely characterised by ^{210}Pb deficits $((^{210}Pb/^{226}Ra)_0 < 1)$, though four of

376   the samples lie within error of secular equilibrium. Figs. 1b and c show $(^{210}Pb/^{226}Ra)_0$ ratios

377   during different stages of the 2006 and 2010 eruptions, respectively. The 2006 samples show

378   very little variation throughout the eruption, with most samples showing ^{210}Pb deficits. The

379   sample erupted towards the end of the eruptive period lies within error of secular equilibrium.

380   For the 2010 rocks, the LGD-Inc sample (M11-28b), representing the onset of the 2010

381   eruption (26 October; Stage 2) shows a significant ^{210}Pb deficit $((^{210}Pb/^{226}Ra)_0$ of 0.79). This

382   is followed by a change to near equilibrium $(^{210}Pb/^{226}Ra)$ values for the LGD-Inc and DD

383   samples extruded during the rapid dome growth and destruction period between the 29

384   October to 4 November (Stage 3) and emplaced in Stage 4. The white pumice sample erupted

385   during the latest stages of the climactic phase of 5 November (Stage 6) lies within error of the

386   Stage 4 emplaced samples with a ^{210}Pb deficit of 0.92. The 2010 plagioclase separate from a

387   DD clast, M11-01P, has excess $(^{210}Pb)_i$ with $(^{210}Pb/^{226}Ra)_0 = 1.97 \pm 0.42$ (Table 2).

388

4.3. Sr-Nd-Pb radiogenic isotopes

390   Sr-Nd isotopic ratios have also been determined for selected 2006 and 2010 whole-rock

391   samples and are presented in Table 3 and Fig. 4. The accompanying Pb isotope data are

392   published in Handley et al. (2014) and presented in the inset to Fig. 4a. The $^{87}Sr/^{86}Sr$ and

393    $^{143}Nd/^{144}Nd$ ratios of the 2006 and 2010 samples overlap and lie within the field of previously

394   published data on historically erupted samples from the volcano (Woodhead et al., 2001;

395   Gertisser and Keller, 2003a; Debaille et al., 2006), towards the higher $^{87}Sr/^{86}Sr$, low-

396   intermediate $^{143}Nd/^{144}Nd$-end of the Merapi array, characteristic of the Merapi high-K series

397   volcanic rocks that have erupted since ~1900 ^{14}C years B.P. (Gertisser et al., 2003a) (Fig. 4a).

398   The 2006 and 2010 Pb isotope ratios are indistinguishable from one another and are

399   remarkably similar to Pb isotope ratios determined for both high-K (<1900 ^{14}C yr B.P.) and

400   medium-K (>1900 ^{14}C yr B.P.) Merapi volcanic rocks (Handley et al., 2014) (Table 3; Fig. 4a

401   inset). The 2006, 2010 and previously published Merapi data plot within the range of Th

402   isotopic ratios of other Javanese volcanic rocks (Turner and Foden, 2001) at slightly higher

403   Sr isotopic composition (Fig. 4b). Local Javanese calcareous crustal samples (Gertisser and

404   Keller, 2003a; Gardner et al., 2012; Handley et al., 2014; Fig. 2 caption), a Merapi calc-

405   silicate xenolith sample (Gertisser and Keller, 2003a), I-type Sumatran Granitoids (Gasparon

406   and Varne, 1995) and altered oceanic crust (AOC; Staudigel et al., 1995) have similar Sr

407   isotopic ratios to the Merapi samples but moderate to significantly higher estimated Th

408   isotopic ratios. The Merapi samples have generally higher Th and lower Sr isotopic ratios

409   compared to Indian Ocean pelagic sediments (Ben Othman et al., 1998; Gasparon and Varne,

410   1998), Bulk Java Sediment (Plank and Langmuir, 1998) and the two S-type Sumatran

411   granites, with low Th and high Sr isotopic ratios (Gasparon and Varne, 1995). No

412   correlations are observed between U-series activity ratios and Sr-Nd isotope ratios for the

413   2006 and 2010 samples (e.g., Fig 4b).

414

415   **5. Discussion**

416   As noted in Sections 1 and 2, previous studies of the 2010 Merapi volcanic rocks suggested

417   that rapid ascent of a larger volume of more volatile-rich magma, with the additional

418   potential contribution of CO_2 from the assimilation of carbonate crust was responsible for the

419   more explosive eruption in 2010 compared to 2006 (Surono et al., 2012; Borisova et al.,

420   2013; Costa et al., 2013; Preece et al., 2013; 2014; 2016; Erdmann et al., 2016). These

421   hypotheses can be scrutinised and assessed with the new isotopic data.

422

423   *5.1. Petrogenetic components and timescales of magmatic processes from U-Th-Ra*

424   *disequilibria and radiogenic isotopic compositions*

425   The 2006 and 2010 Merapi volcanic rocks are characterised by ^{238}U excesses (Fig. 2a),

426   typical of subduction-related volcanic rocks, suggesting that recent fluid addition, likely from

427   the down-going slab (e.g., Condomines et al., 1988; Gill and Williams, 1990; Hawkesworth

428   et al., 1997) or that in-growth melting in the mantle and subsequent crustal modification (e.g.,

429   Reubi et al., 2014; Huang et al., 2016), occurred in the last 380 ka. In the past, Th isotopic

430   variation in volcanic rocks (the vertical spread in data on the U-Th equiline diagram) has

431   been used to estimate magma residence or storage times assuming closed-system

432   differentiation (e.g., Heath et al., 1998). However, given the strong evidence for open-system

433   processes, such as magmatic recharge and carbonate assimilation at Merapi volcano (e.g.,

434   Chadwick et al., 2007; Deegan et al., 2010; Borisova et al., 2013; Troll et al., 2013) and

435   Merapi's almost continuous eruptive activity over the past few hundred years (Voight et al.,

436   2000), the limited variation observed in ($^{230}Th/^{232}Th$) ratios in Fig. 2a is likely explained

437   through the combination of magmatic differentiation, magma recharge and the potential

438   assimilation of carbonate material, instead of being attributed to a single process such as

439   closed-system magmatic differentiation (see arrows in Fig. 2a).

440   Crustal assimilation of carbonate material is implicated in petrogenesis at Merapi

441   (e.g., Chadwick et al., 2007, Deegan et al., 2010, Borisova et al., 2013; Troll et al., 2013) and

442   has been proposed by some to play a role in the more explosive behaviour of the 2010

443   eruption (e.g., Borisova et al., 2013; 2016; Troll et al., 2013). A study by Allard et al. (1983)

444   and more recent studies (e.g., Troll et al., 2012) on the $\delta^{13}C$ composition of fumarole gases

445   from Merapi suggest that a high $\delta^{13}C$, non-magmatic CO_2 input may be important, such as

446   that associated with late-stage crustal decarbonation reactions through assimilation of

447   limestone and skarnification processes. Javanese limestone or calcareous marl is expected to

448   have a higher U/Th concentration ratio compared to the Merapi magma (e.g., 0.65 (Handley

449   et al., 2014) relative to 0.22-0.24, respectively, Table 1) and will be older than 380 ka.

450   Carbonate crustal material is therefore, projected to sit on the equiline in Fig. 2 but at higher

451    $(^{238}U/^{232}Th)$ and $(^{230}Th/^{232}Th)$ than the volcanic samples. Using the U and Th concentrations

452   of local Javanese calcareous sediments (Handley et al., 2014; Fig. 2 caption) and chalky lithic

453   clasts found in the 1883 Krakatau eruption deposits (Gardner et al., 2012) and assuming that

454    $(^{238}U/^{232}Th)$ is in secular equilibrium, the local calcareous sedimentary crust would have

455    $(^{238}U/^{232}Th)$ (and also therefore, $(^{230}Th/^{232}Th)$ ratios) of between 0.85 and 1.98 (Fig. 2). The

456   arrows on Fig. 2a show the expected impact on the activity ratios from the addition of such

457   carbonate material. The 2010 Merapi data are relatively scattered in $(^{238}U/^{232}Th)$-

458    $(^{230}Th/^{232}Th)$ space and therefore, it is not possible to rule out the influence of carbonate

459   assimilation in the more recent explosive eruption. However, calc-silicate xenoliths were

460   found in the 2006 and 2010 volcanic deposits (e.g., Borisova et al., 2016) and therefore, due

461   to the overlap in U-series isotopic composition of the 2006 and 2010 samples, it is deemed

462   unlikely that a greater amount of carbonate assimilation was implicated in the 2010 eruption

463   based on the U-series data and field observations. The Merapi 2006 and 2010 Sr-Nd-Pb

464   radiogenic isotopic compositions show no difference between eruptions, or in the case of Pb

465   isotopes, with previous eruption periods (Fig. 4a), therefore, again it is considered unlikely

466   that there was a greater degree of carbonate assimilation in 2010 compared to 2006 as a

467   primary explanation for the change in explosivity. Furthermore, in a plot of $(^{230}Th/^{232}Th)$

468   activity ratio versus $^{87}Sr/^{86}Sr$ (Fig. 4b) the 2010 Merapi data show no greater predicted

469   influence from local crustal/carbonate material in magma genesis compared to 2006 and

470   other Javanese volcanic rocks.

471   As carbonate crustal material will be significantly older than 8000 years (5 times the
472 half-life of ^{226}Ra) it is expected to have $(^{226}$Ra$/^{230}$Th$) = 1$, i.e. to be in secular equilibrium.
473 Local limestone/calcareous marl crust is also characterised by significantly lower SiO_2
474 content compared to the Merapi volcanic rocks (Handley et al., 2014), therefore, bulk
475 assimilation of limestone by magma would lead to a shift to lower SiO_2 and $(^{226}$Ra$/^{230}$Th$)$. In
476 contrast, addition of fluid produced from skarnification processes would lead to a shift to
477 lower SiO_2 and higher $(^{226}$Ra$/^{230}$Th$)$, presuming that the fluid/solid partition coefficients for
478 Ra are greater than those for Th for this process. Magmatic recharge would be expected to
479 create a shift to higher $(^{226}$Ra$/^{230}$Th$)$ at constant or variable SiO_2, depending on the SiO_2
480 composition of the recharging magma (Fig. 5). Assimilation of older igneous crust (older
481 than 8000 years and therefore, in secular equilibrium) of similar composition to the present
482 day Merapi volcanic rocks, would significantly reduce the $(^{226}$Ra$/^{230}$Th$)$ of the samples with
483 little change in SiO_2 if completely digested. Partial melting of igneous crust could add
484 siliceous material with ^{226}Ra excesses or deficits depending on the residual mineralogy.
485 These processes may create scatter in data on a $(^{226}$Ra$/^{230}$Th$)$ versus SiO_2 plot, which may
486 have traditionally been interpreted as a timescale for closed-system differentiation (Fig. 5).
487 Therefore, as recharge and assimilation are both implicated for Merapi, changes in
488 $(^{226}$Ra$/^{230}$Th$)$ are not likely representative of closed-system evolution timescales as was also
489 found at Lopevi volcano in the Vanuatu arc (Handley et al., 2008). The 2006 and 2010
490 volcanic rocks appear to display different trends in Fig. 5. The 2006 sample suite shows a
491 near vertical trend with a slight increase in SiO_2 content with decreasing $(^{226}$Ra$/^{230}$Th$)$, which
492 could be interpreted as magmatic differentiation or recharge/assimilation of older igneous
493 material, and the 2010 suite displays a positive correlation between SiO_2 and $(^{226}$Ra$/^{230}$Th$)$,
494 which could be attributed to bulk carbonate assimilation (see vectors in Fig. 5). However,
495 these observations are largely dependent on the lowermost $(^{226}$Ra$/^{230}$Th$)$ sample in each
496 eruption suite as the majority of samples show similar $(^{226}$Ra$/^{230}$Th$)$ ratios. As the U-Th and
497 radiogenic isotopic ratios show little difference between the 2006 and 2010 eruptions (i.e.,
498 pointing to a similar source composition for both), the relatively lower SiO_2 content of the
499 2010 rocks compared to the 2006 rocks is consistent with a more mafic recharge magma that
500 underwent faster ascent/less stalling in the crust (e.g., Surono et al., 2012; Costa et al., 2013;
501 Nadeau et al., 2013; Preece et al., 2013; Borisova et al., 2016) and that may have mixed with
502 a magma compositionally similar to that erupted in 2006.

503

504 *5.2. Timing of fluid addition and crystallisation (last fractionation of Ra-Th)*

505   As noted above, the Merapi volcanic rocks all have excess ^{226}Ra, relative to its parent nuclide

506   ^{230}Th (Fig. 2), which in arc rocks is commonly attributed to fluid addition from the

507   subducting slab within the last ~8000 years (e.g., Turner and Hawkesworth, 1997; Turner et

508   al., 2001, 2003, cf. Huang et al., 2008; 2016). At Merapi, there is clear evidence for

509   assimilation of carbonate rocks during differentiation (e.g., Costa et al., 2013; Nadeau et al.,

510   2013; Troll et al., 2013; Borisova et al., 2016). One of these lines of evidence is the presence

511   of abundant calc-silicate xenoliths in Merapi lavas (e.g., Gertisser and Keller, 2003a; Troll et

512   al., 2013). In addition, Merapi whole-rock, grain and in-situ feldspar oxygen isotope data

513   suggest that contamination at shallow levels involves a high δ^{18}O component, such as

514   carbonate crust (Troll et al., 2013; Borisova et al., 2016) rather than a low δ^{18}O component,

515   such as hydrothermal fluid. Thus, we postulate that at least part of the enrichments in Ra

516   observed for Merapi magmas may result from fluid transfer from carbonates included within

517   the magma and in the magma chamber walls as they were transformed into calc-silicates

518   (skarns). This carbonate imprint is likely superimposed upon magma compositions already

519   characterised by ^{226}Ra excess. Published Merapi (^{228}Ra/^{232}Th) ratios lie within error of

520   secular equilibrium (Gauthier and Condomines, 1999) and imply that any Ra enrichment to

521   Merapi magmas occurred >30 years before eruption, due to the short half-life of ^{228}Ra (5.75

522   yrs).

523   The plagioclase crystal separates from the 2006 and 2010 samples have (^{238}U/^{232}Th)

524   and (^{230}Th/^{232}Th) ratios that lie within the range displayed by the whole rock ratios (Table 1),

525   suggesting that older recycled crystals do not dominate the plagioclase population (cf. van

526   der Zwan et al., 2013). However, plagioclase phenocrysts from Merapi are noteworthy for the

527   abundance of glass inclusions (e.g., Costa et al., 2013). Thus, the similarity in U-Th nuclide

528   abundances between plagioclase separates and whole rocks likely reflects domination of the

529   U-Th budgets in plagioclase crystals by the inclusions, and we cannot rule out that some

530   plagioclase cores have ages that are long compared to the half life of ^{230}Th. In contrast,

531   plagioclase crystal separates from lavas erupted in both years have similar levels of ^{226}Ra

532   excesses over ^{230}Th (Fig. 2b), which are slightly higher than the whole-rock observed ^{226}Ra

533   excesses. The 2010 dense dome plagioclase sample (M11-01P; Table 2) also has excess ^{210}Pb

534   ((^{210}Pb/^{226}Ra)$_0$ = 1.97). As Pb is more compatible than Ra in plagioclase (e.g., Reagan et al.,

535   2008), the ^{210}Pb excess indicates that some plagioclase in Merapi volcanic rocks grew within

536   decades of eruption. Similar to that observed for highly porphyritic andesites from Mount St.

537   Helens (Reagan et al., 2008) and Arenal (Reagan et al., 2006). This timeframe concurs with

538   estimated plagioclase growth and residence timescales of <34 years for the 2010 eruption

539   given by Borisova et al. (2016) and largely with timescales of Merapi plagioclase crystal

540   growth of 5 to 310 years determined by van der Zwan et al. (2013).

541

542   *5.3. Timescales of degassing and magma ascent from ^{210}Po- ^{210}Pb-^{226}Ra disequilibria*

543   In contrast to other magmatic systems that exhibit complete, or almost complete, loss of ^{210}Po

544   ($t_{1/2}$ = 138.4 days) on eruption (e.g., Arenal: Gill et al., 1985, Reagan et al., 2006; Mount St.

545   Helens: Reagan et al., 2008), the 2010 Merapi rocks were variably degassed of ^{210}Po upon

546   eruption (Fig. 3), showing no systematic temporal evolution. The light grey dense inclusion

547   (LGD-Inc) clasts from Stage 2 (M11-28b) and Stage 4 (M11-05) were the least degassed of

548   ^{210}Po on eruption (Table 2). Preece et al. (2016) have suggested that these inclusions

549   represent parts of a plug in the shallow conduit and the initial intrusion into the shallow

550   magma plumbing system prior to eruption. Therefore, the magma forming the inclusions may

551   have stalled at a shallow level and cooled below the blocking temperature for degassing Po

552   for a period that was long enough to allow Po to ingrow via radioactive decay from its

553   nuclide parent prior to eruption. If we assume that these samples would have been fully

554   degassed of Po on ascent before reaching the shallow conduit, i.e. had no initial ^{210}Po, the

555   time to rebuild the observed Po by decay from the parent nuclide would be ~53-74 days

556   before eruption. If these samples had initial (^{210}Po/^{210}Pb) ratios of 0.26-0.31 (Table 2), Po

557   ingrowth calculations would suggest that the plug cooled to below the blocking temperature

558   for degassing Po between 29-56 days before it erupted. Therefore, initial intrusion of magma

559   is estimated to have taken place several weeks to several months prior to the onset of the

560   main eruption period. This time frame largely corresponds to a marked increase in all

561   monitored parameters: ground inflation, earthquake counts and seismic energy release from

562   20 September 2010, and a significant increase in temperature, CO_2/SO_2 and H_2S/SO_2 ratios,

563   in summit fumaroles from the end of September, which suggested a shift to a deep degassing

564   source, attributed to the influx of new magma (Surono et al., 2012). In contrast to the LGD-

565   Inc sample from Stage 4, the DD samples (M11-27-5 and M11-12) from the same eruptive

566   phase have degassed most, if not all, of their Po at the time of eruption. This suggests that

567   despite prior evidence for rapid ascent of the 2010 dome-forming magma, for example, the

568   lack of amphibole breakdown rims (Costa et al., 2013; Preece et al., 2014) and from microlite

569   textural and compositional analysis (Preece et al., 2014; 2016), the magma was still able to

570   efficiently degas and partition Po into the exsolving gas as it ascended to the surface. Le

571   Cloarec and Gauthier (2003) have shown that gases emitted from previously growing domes

at Merapi are strongly depleted in the most volatile isotopes and gas species. The white pumice from the post-climatic phase of the eruption (M11-18, Stage 6) was 83% degassed of ^{210}Po on eruption; less degassed relative to the DD samples from Stage 4. The samples were leached prior to analysis and therefore, it is unlikely that this is due to Po condensing on vesicle walls prior to or during eruption. Instead, it may reflect less efficient degassing by this stage of the eruption related to fast magmatic ascent. This is in agreement with microlite textures in the white pumice that indicate despite some stalling in the conduit at 1.4-2.4 km depth, the magma experienced fast final ascent during this stage (Preece et al., 2016).

The variation in $(^{210}Pb/^{226}Ra)_0$ measured in the 2006 and 2010 volcanic rocks is comparable to the full range of $(^{210}Pb/^{226}Ra)_0$ reported by Gauthier and Condomines (1999) for rocks erupted between 1981-1995 at Merapi, with most samples showing deficits of ^{210}Pb relative to ^{226}Ra (Fig. 1). This differs with many other arc volcanoes that display values within analytical error of 1 (Reagan et al., 2017). Equilibrium $(^{210}Pb/^{226}Ra)_0$ values in other arc rocks indicate that the last stage of ^{222}Rn degassing must have occurred over a time period short enough to be undetectable using ^{210}Pb-^{226}Ra disequilibria (~less than two years) prior to eruption. In contrast, excess ^{210}Pb is observed in tephra from the cataclysmic eruption of Mount Pinatubo in 1991 that did not significantly vent gases at the surface prior to eruption, and is attributed to ^{210}Pb accumulation in recharging magma at the base of the dacitic Pinatubo reservoir and subsequent mixing (Kayzar et al., 2009). At Merapi, the ^{210}Pb deficits are consistent with the observed evidence for continuous degassing at fumarole fields and through cracks within the dome at Merapi (Le Cloarec and Gauthier, 2003). However, Ra enrichment (relative to ^{210}Pb) can lead to ^{210}Pb deficits if late-stage fluids derived from carbonate skarnification are added to magmas within decades of eruption. ^{210}Pb-^{226}Ra disequilibria may also be affected by the interaction of magma with sulphide melt and brine, which has been suggested for Merapi (e.g., Le Cloarec and Gauthier, 2003; Nadeau et al., 2013; Preece et al., 2014). However, it would be expected that the transfer of sulphide melt or chloride brine from the recharge mafic magma to the shallower magmatic system should largely produce ^{210}Pb excesses, which are not observed in the rocks.

What is clear from the new data is that there is a significant range in $(^{210}Pb/^{226}Ra)_0$ within a single eruption at Merapi, therefore, process interpretations based on one sample per eruption/year may not yield sufficient information about the plumbing system and degassing behaviour over decadal timescales (cf. Gauthier and Condomines, 1999). Berlo et al. (2006) also observed variability in $(^{210}Pb/^{226}Ra)_0$ within a single eruption at Mount St. Helens and attributed it to tapping magma from various depths. Mineral and mineral-melt

606 thermobarometry studies on the 2006 and 2010 Merapi samples suggest that for both
607 eruptions, magmatic crystallisation (and inferred storage) occurs over a range of depths, from
608 ~30 km deep to the surface (Costa et al., 2013; Preece et al., 2014). Recent phase equilibrium
609 experiments conducted by Erdman et al. (2016) suggest Merapi's pre-eruptive main reservoir
610 is located at a depth of $\geq 4.5\text{-}9 \pm 3$ km, which is recharged by a higher temperature magma
611 with a higher melt H_2O content from below. Therefore, it is possible that the variability in
612 $(^{210}Pb/^{226}Ra)_0$ within single eruptions at Merapi is related to variation in magmatic source
613 depth, and mixing of a faster moving, more undegassed, recharging magma with slower
614 moving, shallower, more degassed magma as well as any influence from late-stage carbonate
615 assimilation.

616 The 2006 scoria samples are characterised by deficits of ^{210}Pb, with all samples
617 (except one) lying outside of error of secular equilibrium with no clear evolutionary trend in
618 $(^{210}Pb/^{226}Ra)_0$ (Fig. 1). Assuming the simplest model of efficient (complete) removal of ^{222}Rn
619 with other exsolving gas species (e.g. H_2O, CO_2, SO_2), that the influence of carbonate
620 assimilation is similar for all samples, and a system closed to magmatic recharge (equation 11
621 of Gauthier and Condomines, 1999), the range of ^{210}Pb deficits observed in the 2006 Merapi
622 samples imply approximately 2-4 years (with one sample giving 7 years) of degassing prior
623 to eruption (Table 2). This timeframe compares well with maximum timescale estimates
624 using Fe-Mg gradients in 2006 clinopyroxenes of 2.4-5 years for magma influx into
625 intermediate or shallow depth reservoirs prior to eruption (Costa et al., 2013). The agreement
626 between the two approaches suggests that radon degassing from this shallow reservoir may
627 be the dominant process controlling the ^{210}Pb systematics in Merapi rocks. The first signs of
628 activity for the 2006 eruption were detected by seismic and deformation data in July 2005,
629 which may suggest that the magma may have been degassing while ascending from deeper
630 levels for a year or two before its movement to a shallow level storage region was seismically
631 detected. The previous eruption prior to 2006, occurred 5 years earlier in 2001, so the
632 interpretation of a new influx of magma from a deeper region after 2001 is also compatible
633 with Merapi's eruptive history.

634 Despite differences in initial ^{210}Po between the scoria (S2S M11-28a) and light grey
635 inclusion (LGD-Inc M11-28b) samples erupted during the Stage 2 of the eruption on the 26
636 October, both samples appear to have significantly lower initial ^{210}Pb activities of around 2.3-
637 2.5 dpm/g compared to the other 2010 samples (Fig. 3). This suggests that magma involved
638 in the initial eruption had degassed for longer and either that the magma was sourced from a
639 greater depth and/or travelled more slowly to the surface compared with later stages of the

19

640   eruption. Microlite textures in the rocks suggest that the eruption intensity and decompression

641   rates were faster for Stage 4 and 6 samples compared to Stage 2 (Preece et al., 2016) and

642   therefore, a slower ascent to the surface is the likely explanation for the lower ^{210}Pb activities

643   in Stage 2 samples. The ^{210}Pb deficit of the LGD-Inc (M11-28b) erupted at the start of the

644   2010 eruption on 26 October can be modelled by 8 years of continuous degassing (equation

645   11 of Gauthier and Condomines, 1999; Table 2) prior to emplacement at shallow levels

646   around a month or two prior to the eruption (calculated from the initial ^{210}Po activity). The

647   explosive activity at the start of the eruption on 26 October was accompanied by significant

648   release of SO_2 (Surono et al., 2012; Fig. 1c) and so, as such a large ^{210}Pb deficit is recorded in

649   the inclusion, it is unlikely that a significant volume of this gas was trapped for an amount of

650   time that was long relative to the half-life of ^{222}Rn in the shallow magma system because the

651   decay of ^{222}Rn would have increased the ^{210}Pb activity.

652   The eruption in 2006 was 4 years prior to 2010, suggesting that magma that formed

653   the light grey material may represent slowly ascending, unerupted magma related to

654   magmatic influx from the 2006 magmatic event, as the ^{210}Pb deficits from the 2006 samples

655   suggest between 2-4 years of degassing prior to eruption, giving a total of 6-8 years of

656   degassing for this material. Between 1 and 4 November 2010 in the main dome-building

657   phase (Stage 3, with samples emplaced in PDC deposits during Stage 4), the three samples

658   analysed show small ^{210}Pb deficits to a small ^{210}Pb excess and lie within error of secular

659   equilibrium. This likely represents the arrival of relatively fast moving magma that did not

660   stall and degas for any significant amount of time since its last stagnation point. The rapid

661   ascent of this relatively undegassed magma triggered a sudden release of gas close to the

662   surface, which caused the massive SO_2 flux during the climactic stage (Fig. 1). This

663   interpretation is consistent with previous petrological studies on minerals and melt inclusion

664   work that suggest the supply of a greater volume of volatile-rich, deeper magma in 2010, that

665   ascended fast with little time to degas (Costa et al., 2013; Preece at al., 2013, 2014). For

666   example, maximum times for magma influx prior to eruption estimated from Fe-Mg gradients

667   in clinopyroxenes give shorter timescales for 2010 compared to the 2006 eruption, of 1.6-2.7

668   years relative to 2.4-5 years, respectively (Costa et al., 2013). The white pumice sample

669   erupted during the latest stages of the climatic phase of 5 November (Stage 6) has a slight

670   ^{210}Pb deficit but lies within error of the Stage 4 samples, also suggesting relatively rapid

671   magmatic ascent. Preece et al. (2014) have shown that clinopyroxene in the white pumice

672   samples crystallised from the deeper levels of the plumbing system, suggesting an increase in

673   deep magma supply at this stage of the eruption. The larger size, lower number density and

674   equant morphologies of microlites in the white pumice, compared to those in samples from

675   other stages of the eruption, suggest that this magma stalled in the conduit at estimated depths

676   of ~1.4-2.4 km prior to a rapid final ascent to the surface (Preece et al., 2016).

677   Gauthier and Condomines (1999) (grey diamonds Fig. 1) explained the variation

678   observed in $(^{210}Pb/^{226}Ra)_0$ in rocks erupted between 1981 and 1995 by short periods (<10

679   years) of closed-system evolution and continuous magmatic degassing. They attributed

680   higher $(^{210}Pb/^{226}Ra)_0$ ratios to reinjections of magma and noted that the higher $(^{210}Pb/^{226}Ra)_0$

681   ratios coincided with explosive gravitational dome collapses in 1984 and 1992. In this study,

682   the generally higher $(^{210}Pb/^{226}Ra)_0$ observed in samples erupted between 1 to 4 Nov 2010,

683   compared to the more effusive 2006 eruption, supports the model by Gauthier and

684   Condomines (1999) that periods of magmatic recharge are linked to rapid dome extrusion

685   and, ultimately, more explosive eruptions at Merapi and the low/zero initial Po activities in

686   these samples suggest that open-system degassing must have occurred very shortly, in the

687   weeks to months, before eruption.

688

689   **6. Conclusions**

690   The main conclusions from this study are presented schematically in Fig. 6 and are as

691   follows:

692   1. The similar U-Th-Ra and Sr-Nd-Pb isotopic ratios presented by the 2006 and 2010

693   Merapi volcanic rocks, along with the presence of calc-silicate xenoliths in both the

694   2006 and 2010 eruption deposits, suggest that although carbonate crustal assimilation

695   must have played some role in magmatic evolution for both eruptions it is not a

696   significant contributor to the transition in the volcano's explosive style. Evidence for

697   magmatic recharge and crustal assimilation at Merapi means that U-Th-Ra

698   disequilibria cannot be interpreted using a closed-system evolution timescale model.

699   At present, it is unclear whether Ra excesses are fully attributed to fluid addition from

700   the subducting slab or whether Ra is also added by fluids produced from skarn

701   formation over a timeframe of hundreds to several thousand years prior to eruption

702   (Fig. 6 (A)).

703   2. The repeated measurement of (^{210}Po) activities for samples collected shortly after

704   eruption reveals that sample MER061406-D was not a juvenile fragment of the 2006

705   eruption and shows that the juvenile 2006 and 2010 samples were all depleted in

706   ^{210}Po, relative to ^{210}Pb, at the time of eruption but were variably degassed (Fig. 6 (C)).

707   In the 2010 samples, the degree of ^{210}Po degassing is directly related to sample texture

708   and eruption phase, with the greatest degree of degassing observed in the dense dark

709   dome-building samples erupted during the climatic phase of the eruption (97-100% of

710   ^{210}Po degassed on eruption) and the lowest degree of degassing measured in the light

711   grey inclusions (69-74% of ^{210}Po degassed on eruption) from the initial and earlier

712   phases of the eruption. The light grey inclusion samples are interpreted to represent an

713   initial influx of magma into the shallow plumbing system (Preece et al., 2016). If this

714   is the case, Po ingrowth calculations suggest that the initial intrusion 'plug' cooled

715   through the blocking temperature several weeks to several months before eruption,

716   which is consistent with the marked increase in observed monitoring parameters from

717   20 September 2010 onwards that suggested influx of new magma from deep.

718   3. This study shows that there is a wide range in $(^{210}Pb/^{226}Ra)_0$ observed in volcanic

719   deposits from single eruptive episodes at Merapi, which are comparable to the entire

720   range in $(^{210}Pb/^{226}Ra)_0$ ratios for rocks erupted between 1981-1995 (Gauthier and

721   Condomines, 1999). Using a model of complete radon degassing, the ^{210}Pb-^{226}Ra

722   disequilibria can be modelled by ~2-4 years and ~0-3 years of degassing prior to

723   eruption in 2006 and 2010, respectively (Fig. 6 (B)). These timeframes correlate well

724   with maximum timescale estimates from Fe-Mg compositional heterogeneities in

725   clinopyroxene, which suggest 2.4-5 years (2006 eruption) and 1.6-2.7 years (2010

726   eruption) between magma influx into intermediate/shallow depth reservoirs and

727   eruption (Costa et al., 2013). The agreement in timescales using different approaches

728   suggests that despite the potential impact of crustal assimilation on $(^{210}Pb/^{226}Ra)$

729   ratios, magmatic degassing and recharge alone can explain ^{210}Pb-^{226}Ra disequilibria in

730   Merapi volcanic rocks. In this context, the ^{210}Pb data suggest that the deeper magma

731   involved in the 2010 eruption began degassing only shortly before eruption (possibly

732   due to its rapid ascent). This interpretation is supported by the lack of amphibole

733   reaction rims in 2010 deposits along with microlite textural and compositional

734   analysis, which suggest minimal storage and relatively rapid movement of the 2010

735   magma relative to that erupted in 2006 (Preece et al., 2013; 2014; 2016). It also

736   corroborates the work of Gauthier and Condomines (1999), suggesting that periods of

737   magmatic recharge are linked to rapid dome extrusion and ultimately, more explosive

738   eruptions at Merapi. Excess ^{210}Pb relative to ^{226}Ra in plagioclase from the 2006 and

739   2010 volcanic rocks indicates that part of the plagioclase in Merapi volcanic rocks

740   grew within decades of eruption.

741

7. Acknowledgements

Figure Captions

Figure 1. a) Initial (^{210}Pb/^{226}Ra)$_0$ activity ratios of the 2006 and 2010 Merapi volcanic rocks (this study) compared to the (^{210}Pb/^{226}Ra)$_0$ activity ratios for Merapi volcanic rocks erupted between 1981 to 1995 (Gauthier and Condomines, 1999; grey diamonds). Panels b) and c) show the detailed changes in (^{210}Pb/^{226}Ra)$_0$ activity ratios throughout the 2006 and 2010 eruptions, respectively. COSPEC SO$_2$ flux measurements for the 2006 eruption (grey circles in panel b are from the Geological Agency Center for Volcanology and Geological Hazard Mitigation (http://www.vsi.esdm.go.id/index.php/gunungapi/data-dasar-gunungapi/542-g-merapi?start=5) and the maximum flux during 1992-2007 (dashed line in b) and mean SO$_2$ gas flux data for the 2010 eruption are from Surono et al. (2012).

Figure 2. a) (^{238}U/^{232}Th)-(^{230}Th/^{232}Th) equiline diagram for Merapi volcanic rocks and plagioclase separates. Arrows show the expected impact on whole-rock compositions from: i) magmatic recharge (a likely shift to lower (^{230}Th/^{232}Th) relative to differentiated magma), ii) assimilation of older volcanic material in secular equilibrium (with a similar U/Th elemental ratio to the 2006 and 2010 samples) and/or closed system differentiation (shift to higher (^{230}Th/^{232}Th)), and iii) the potential assimilation of crustal carbonate material (a shift towards the equiline but at significantly higher (^{238}U/^{232}Th)). The vector for carbonate assimilation is estimated using the U and Th concentrations of local Javanese calcareous sediments (data given in Handley et al., 2014 and local upper crust samples MX99-1: U: 1.36 ppm, Th: 4.64 ppm; MX99-2: U: 0.72 ppm, Th: 2.56) and assuming that (^{238}U/^{232}Th) is in secular equilibrium. Previously published whole-rock Merapi data (historical and recent ($\leq$ 200 years

23

776 old) and older) from Gill and Williams (1990), Gauthier and Condomines (1999) and Turner

777 and Foden (2001), Condomines et al. (2005). b) $(^{230}Th/^{238}U)$-$(^{226}Ra/^{230}Th)$ diagram for

778 Merapi volcanic rocks and plagioclase separates. Previously published whole-rock Merapi

779 data from Gill and Williams (1990), Gauthier and Condomines (1999), and Condomines et al.

780 (2005). The 'older' Merapi data of Condomines et al. (2005) and the Turner and Foden

781 (2001) data were not used in Fig. 2b due to either i) uncertainty in the eruption age of the

782 sample or, ii) samples had assumed, and not measured, $(^{230}Th/^{232}Th$ ratios).

783

784 Figure 3. Plot of ^{210}Po activities versus days since eruption for leached Merapi whole-rock

785 volcanic samples. Note that only two of the 2006 samples were analysed in the days (rather

786 than years) following the eruption. The 2006 sample, MER061406-D, has high initial ^{210}Po

787 and is therefore, not a juvenile fragment of the 2006 eruption. For the 2006 samples that were

788 more than two years old at the time of measurement ('other 2006'), i.e. five times the half-life

789 of ^{210}Po (138.4 days), (^{210}Pb) was considered equal to (^{210}Po) and these samples are plotted

790 on the right-hand y-axis (plotted arbitrarily at 1000 days) for comparison of initial (^{210}Pb)

791 activities. Indicated initial (^{210}Po) and (^{210}Pb) values (Table 2) were obtained through a

792 Markov Chain Monte Carlo simulation using Matlab (see Section 3). Error bars represent 2σ

793 total analytical error. Refer to Table 1 and the text for further eruption framework details and

794 clast type information.

795

796 Figure 4. a) $^{87}Sr/^{86}Sr$ versus $^{143}Nd/^{144}Nd$ for the 2006 and 2010 Merapi volcanic rocks.

797 Previously published Merapi data (grey-filled diamonds) from Debaille et al. (2006),

798 Gertisser and Keller (2003a) and Woodhead et al. (2001). Java (including Krakatau) volcanic

799 rock data (grey crosses) from Edwards et al. (1993), Gerbe et al. (1992), Handley et al. (2007:

800 2008; 2010; 2011), Sendjaja et al. (2009), Turner and Foden (2001), Vukadinovic and

801 Sutawidjaja (1995), White and Patchett (1984), Woodhead et al. (2001). Inset shows Pb

802 isotopic ratios for the 2006 and 2010 Merapi volcanic rocks relative to recent high-K (<1900

803 ^{14}C yr B.P.) and medium-K (>1900 ^{14}C yr B.P.) Merapi volcanic rocks (green triangles)

804 (Handley et al., 2014). b) $(^{230}Th/^{232}Th)$ versus $^{87}Sr/^{86}Sr$ for the 2006 and 2010 Merapi

805 volcanic rocks. The $(^{230}Th/^{232}Th)$ activity ratios for all samples, except the volcanic rock

806 samples from Merapi and Java were calculated using their U and Th concentrations and

807 assuming that $(^{238}U/^{232}Th)$ is in secular equilibrium. Previously published Merapi data from

808 Turner and Foden (2001). Java volcanic rock field (Galunggung and Krakatau) from Turner

24

809   and Foden (2001). Java calcareous crustal data and Merapi calc-silicate xenolith data from

810   Gardner et al. (2012), Gertisser and Keller (2003a), Handley et al. (2014). Bulk Java

811   subducted sediment, Bulk Sumatra subducted sediment and Bulk East Sunda subducted

812   sediment from Plank and Langmuir (1998). Indian Ocean sediments (pelagic: I-Pelag and

813   terrigeneous: I- Terrig) from Ben Othman et al. (1989), Gasparon and Varne (1998) and

814   Plank and Langmuir (1998). Sumatran Granitoids divided into I-type (low Sr isotopic ratio

815   and moderate to high Th isotopic ratio) and S-type (high Sr isotopic ratio and low Th isotopic

816   ratio) from Gasparon and Varne (1995). Altered oceanic crust (AOC) lies off the top of the

817   diagram at significantly higher Th isotopic ratios ((^{230}Th/^{232}Th) = 8.78 to 53.4) (Staudigel et

818   al., 1995). Inset diagram shows a close up view of the Merapi and Java volcanic data.

819

820   Figure 5. (^{226}Ra/^{230}Th) activity ratio versus SiO_2 (wt%) in Merapi volcanic rocks for the 2006

821   and 2010 eruptions. SiO_2 contents are taken from Preece et al. (2013) and Preece (2014) and

822   are given in Table 1. Previously published Merapi data are from Condomines et al. (2005).

823   Arrows show the expected impact on whole-rock compositions from: i) magmatic recharge or

824   addition of fluid produced by skarn formation (carb. fluid), ii) assimilation of older volcanic

825   material in secular equilibrium with similar SiO_2 content to the 2006 and 2010 samples

826   and/or closed system differentiation and iii) the potential assimilation of crustal carbonate

827   material (a shift towards secular equilibrium and lower SiO_2 content).

828

829   Figure 6. Schematic diagram showing the uranium isotope activity ratios used and the

830   timescales of magmatic processes that have been deduced for the 2006 and 2010 eruptions at

831   Merapi. A: ^{226}Ra and ^{238}U excesses indicate addition of ^{226}Ra on a timescale of 8000 years or

832   less and for ^{238}U on a timescale of <380,000 years, probably due to fluid addition from the

833   subducting slab. It is unconstrained at present whether crustal assimilation of carbonate

834   material or skarn formation processes have added additional ^{226}Ra and ^{238}U to the magma. B:

835   Shallow degassing of ^{222}Rn occurred ~2-4 years prior to eruption in 2006 and ~0-3 years in

836   2010, suggesting that the ascent of volatile-rich magma shortly before eruption contributed to

837   the greater explosivity observed in 2010. C: Final magma ascent and shallow-level

838   emplacement took place over the weeks to months preceding the eruption as indicated by the

839   degassing of ^{210}Po.

840

841   **References**

842   Allard P. (1983) The origin of hydrogen, carbon, sulphur, nitrogen and rare gases in volcanic
843   exhalations; evidence from isotope geochemistry. In: Tazieff, H. and Sabroux, J. (eds).
844   *Forecasting Volcanic Events*. Elsevier, New York, pp.337–386.

845   Andreastuti S. D., Alloway B. V. and Smith I. E. M. (2000) A detailed tephrostratigraphic
846   framework at Merapi volcano, Central Java, Indonesia: implications for eruption
847   predictions and hazards assessment. *J. Volcanol. Geotherm. Res.* **100**, 51-67.

848   Bennett J. T., Krishnaswami I. S., Turekian K. K., Melson W. G. and Hopson C. A. (1982)
849   The uranium and thorium decay series nuclides in Mt. St. Helens effusives. *Earth*
850   *Planet.Sci. Lett.* **60**, 61-69.

851   Ben Othman D. B., White W. M. and Patchett J. (1989) The geochemistry of marine
852   sediments, island arc magma genesis, and crust-mantle recycling. *Earth Planet. Sci.*
853   *Lett.* **94**: 1-21.

854   Berlo K. and Turner S. (2010) ^{210}Pb–^{226}Ra disequilibria in volcanic rocks. *Earth Planet. Sci.*
855   *Lett.* **296**, 155-164.

856   Berlo K., Turner S., Blundy J., Black S. and Hawkesworth C. (2006) Tracing pre-eruptive
857   magma degassing using (^{210}Pb/^{226}Ra) disequilibria in the volcanic deposits of Mount St.
858   Helens. *Earth Planet. Sci. Lett.*, **249**, 337-349.

859   Bourdon B., Ribe N. M., Stracke A., Saal A. E. and Turner S. P. (2006) Insights into the
860   dynamics of mantle plumes from uranium-series geochemistry. *Nature* **444**, 713-717.

861   Birck J. L. (1986) Precision K-Rb-Sr isotope analysis-application to Rb-Sr chronology.
862   *Chem. Geol.* **56**, 73–83.

863   Borisova A. Y., Martel C., Gouy S., Pratomo I., Sumarti S., Toutain J.-P., Bindeman I. N., de
864   Parseval P., Metaxian J.-P. and Surono (2013) Highly explosive 2010 Merapi eruption:
865   Evidence for shallow-level crustal assimilation and hybrid fluid. *J. Volcanol.*
866   *Geotherm. Res.* **261**, 193-208.

867   Borisova A. Y., Gurenko A. A., Martel C., Kouzmanov K., Cathala A., Bohrson W. A.,
868   Pratomo I. and Sumarti S. (2016) Oxygen isotope heterogeneity of arc magma recorded
869   in plagioclase from the 2010 Merapi eruption (Central Java, Indonesia). *Geochim.*
870   *Cosmochim, Acta* **190**, 13-34.

871   Bragagnia A., Avanzinelli R., Freymuth H. and Francalanci L. (2014). Recycling of crystal
872   mush-derived melts and short magma residence times revealed by U-series disequilibria
873   at Stromboli volcano *Earth Planet. Sci. Lett.* 404: 206–219.

874   Camus G., Gourgoud A., Mossand-Berthommier P.-C., and Vincent P.-M. (2000) Merapi
875   (Central Java, Indonesia): An outline of the structural and magmatological evolution,

876   with special emphasis to the major pyroclastic events. *J. Volcanol. Geotherm. Res.* **100**,

877   139-163.

878   Chadwick J. P., Troll V. R., Ginibre C., Morgan D., Gertisser R., Waight T. E. and Davidson

879   J. P. (2007) Carbonate assimilation at Merapi Volcano, Java, Indonesia: Insights from

880   crystal isotope stratigraphy. *J. Petrol.* **48**, 1793-1812.

881   Charbonnier S.J. and Gertisser R. (2008) Field observations and surface characteristics of

882   pristine block-and-ash flow deposits from the 2006 eruption of Merapi volcano, Java,

883   Indonesia. *J. Volcanol. Geotherm. Res.* **177**, 971-982.

884   Charbonnier S. J. and Gertisser R. (2011) Deposit architecture and dynamics of the 2006

885   block-and-ash flows of Merapi Volcano, Java, Indonesia. *Sedimentology* **58**, 1573-

886   1612.

887   Charbonnier S. J., Germa A. M., Connor C. B., Gertisser R., Preece K., Komorowski J.-C.,

888   Lavigne F., Dixon T. H. and Connor L. J. (2013) Evaluation of the impact of the 2010

889   pyroclastic density currents at Merapi volcano from high-resolution satellite imagery

890   analysis, field investigations and numerical simulations. *J. Volcanol. Geotherm. Res.*

891   **261**, 295-315.

892   Condomines M., Gauthier P. J., Tanguy J. C., Gertisser R., Thouret J. C., Berthommier P. and

893   Camus G. (2005) ^{226}Ra or ^{226}Ra/Ba dating of Holocene volcanic rocks: application to

894   Mt. Etna and Merapi volcanoes. *Earth Planet. Sci. Lett.* **230**, 289-300.

895   Condomines M., Gauthier P.-J. and Sigmarsson O. (2003) Timescales of magma chamber

896   processes and dating of young volcanic rocks. In: Bourdon B., Henderson G. M.,

897   Lundstrom C. C., Turner, S. P. (Eds.) *Uranium Series Geochemistry*. Reviews in

898   Mineralogy and Geochemistry. The Mineralogical Society of America, Washington,

899   DC, pp. 125–174.

900   Condomines M., Hemond Ch and Allégre C. J. (1988). U-Th-Ra radioactive disequilibria and

901   magmatic processes. *Earth Planet. Sci. Lett.*, **90**, 243-262.

902   Condomines M., Sigmarsson O. and Gauthier P. J. (2010) A simple model of ^{222}Rn

903   accumulation leading to ^{210}Pb excesses in volcanic rocks. *Earth Planet. Sci. Lett.* **293**,

904   331–338.

905   Costa F., Andreastuti S., de Maisonneuve C. B. and Pallister J. S. (2013) Petrological insights

906   into the storage conditions, and magmatic processes that yielded the centennial 2010

907   Merapi explosive eruption. *J. Volcanol. Geotherm. Res.* **261**, 209-235.

908   Cronin S. J., Lube G., Dayudi D. S., Sumarti S., Subrandiyo S. and Surono (2013). Insights

909   into the October–November 2010 Gunung Merapi eruption (Central Java, Indonesia)

910   from the stratigraphy, volume and characteristics of its pyroclastic deposits. *J.*
911   *Volcanol. Geotherm. Res.* **261**, 244–259.

912 Debaille V., Doucelance R., Weis D. and Schiano P. (2006). Multi-stage mixing in
913   subduction zones: Application to Merapi volcano (Java island, Sunda arc). *Geochim*
914   *Cosmochim Acta* **70**, 723–741.

915 Deegan F. M., Troll V. R., Freda C., Misiti V., Chadwick J. P., McLeod C. L. and Davidson
916   J. P. (2010) Magma-carbonate interaction processes and associated CO_2 release at
917   Merapi volcano, Indonesia: insights from experimental petrology. *J. Petrol.* **51**, 1027-
918   1051.

919 Edmonds, M., and Herd R. A. (2007), A volcanic degassing event at the explosive-effusive
920   transition, *Geophys. Res. Lett.,* **34**, L21310.

921 Edwards C. M. H., Morris J. D. and Thirlwall M. F. (1993). Separating mantle from slab
922   signatures in arc lavas using B/Be and radiogenic isotope systematics. *Nature* **362**, 530-
923   533.

924 Erdmann S., Martel C., Pichavant M., Bourdier J.-L., Champallier R., Komorowski J.-C. and
925   Cholik N. (2016). Constraints from Phase Equilibrium Experiments on Pre-eruptive
926   Storage Conditions in Mixed Magma Systems: a Case Study on Crystal-rich Basaltic
927   Andesites from Mount Merapi, Indonesia. *J Petrol* **57**, 535-560.

928 Gardner M. F., Troll V. R., Gamble J. A., Gertisser R., Hart G. L., Ellam R. M., Harris C. and
929   Wolff J. A. (2012). Crustal Differentiation Processes at Krakatau Volcano, Indonesia.
930   *J. Petrol* **54**, 149-182.

931 Gasparon M. and Varne R. (1995). Sumatran granitoids and their relationship to Southeast
932   Asian terranes. *Tectonophysics* **251**, 277–299.

933 Gasparon M. and Varne R. (1998). Crustal assimilation versus subducted sediment input in
934   west Sunda arc volcanics: an evaluation. *Mineral. Petrol.* **64**, 89–117.

935 Gauthier P-J. and Condomines M. (1999). ^{210}Pb-^{226}Ra radioactive disequilibria in recent lavas
936   and radon degassing: inferences on magma chamber dynamics at Stromboli and Merapi
937   volcanoes. *Earth Planet Sci Lett* **172**, 111-126.

938 Gerbe M.-C., Gouraud A., Sigmarsson O., Harmon R.S., Joron J-L. and Provost A. (1992).
939   Mineralogical and geochemical evolution of the 1982-1983 Galunggung eruption
940   (Indonesia). *Bull Volc* **54**, 284-298.

941 Gertisser R., Charbonnier S.J., Keller J. and Quidelleur X. (2012). The geological evolution
942   of Merapi volcano, Central Java, Indonesia. *Bull Volc* **74**, 1213-1233.

943   Gertisser R. and Keller J. (2003a). Trace element and Sr, Nd, Pb and O isotope variations in
944   medium-K and high-K volcanic rocks from Merapi Volcano, Central Java, Indonesia:
945   evidence for the involvement of subducted sediments in Sunda Arc magma genesis. *J.*
946   *Petrol.* **44**, 457–489.

947   Gertisser R. and Keller J. (2003b). Temporal variations in magma composition at Merapi
948   Volcano (Central Java, Indonesia): magmatic cycles during the past 2000 years of
949   explosive activity. *J. Volc. Geotherm. Res.* **123**, 1–23.

950   Gill, J., Williams, R. and Bruland, K. (1985). Eruption of basalt and andesite lava degasses
951   ^{222}Rn and ^{210}Po. *Geophys Res Lett* **12**, 17–20.

952   Gill, J.B. and Williams, R.W. (1990). Th isotope and U-series studies of subduction-related
953   volcanic rocks. *Geochim Cosmochim Acta* **54**, 1427-1442.

954   Handley H.K., Macpherson C.G., Davidson J.P., Berlo K. and Lowry D. (2007) Constraining
955   fluid and sediment contributions to subduction-related magmatism in Indonesia: Ijen
956   Volcanic Complex, Indonesia. *J. Petrol.* **48**, 1155–1183.

957   Handley H.K., Turner S.P., Smith I.E., Stewart R.B. and Cronin S.J. (2008) Rapid timescales
958   of differentiation and evidence for crustal contamination at intra-oceanic arcs:
959   geochemical and U-Th-Ra-Sr-Nd isotopic constraints from Lopevi volcano, Vanuatu,
960   SW Pacific. *Earth Planet. Sci. Lett.* **273**, 184-194.

961   Handley H.K., Macpherson C.G. and Davidson J.P. (2010) Geochemical and Sr–O isotopic
962   constraints on magmatic differentiation at Gede Volcanic Complex, West Java,
963   Indonesia. *Contrib. Mineral. Petrol.* **159**, 885–908.

964   Handley H.K., Turner S., Macpherson C.G., Gertisser R. and Davidson J.P. (2011) Hf–Nd
965   isotope and trace element constraints on subduction inputs at island arcs: Limitations of
966   Hf anomalies as sediment input indicators. *Earth Planet. Sci. Lett.* **304**, 212–223.

967   Handley H.K., Blichert-Toft J., Gertisser R., Macpherson C., Turner S.P., Zaennudin A. and
968   Abdurrachman M. (2014) Insights from Pb and O isotopes into along-arc variations in
969   subduction inputs and crustal assimilation for volcanic rocks in Java, Sunda arc,
970   Indonesia. *Geochim Cosmochim Acta* **139**, 205–226.

971   Hawkesworth C.J., Turner S.P., McDermott F., Peate D.W. and van Calsteren P. (1997) U-Th
972   Isotopes in Arc Magmas: Implications for Element Transfer from the Subducted Crust.
973   *Science* **276**, 551-555.

974   Holden N.E. (1990). Total half-lives for selected nuclides. *Pure Applied Chem* **62**, 941-958.

975 Huang F., Gao L. and Lundstrom C.C. (2008) The effect of assimilation, fractional
976   crystallization, and ageing on U-series disequilibria in subduction zone lavas. *Geochim*
977   *Cosmochim Acta* **72**: 4136–4145.

978 Huang F., Xu J. and Zhang J. (2016) U-series disequilibria in subduction zone lavas:
979   Inherited from subducted slabs or produced by mantle in-growth melting? *Chem Geol*
980   **440**, 179–190.

981 Jeffery A.J., Gertisser R., Troll V.R., Jolis E. M., Dahren B., Harris C., Tindle A.G., Preece
982   K., O'Driscoll B., Humaida H. and Chadwick J.P. (2013). The pre-eruptive magma
983   plumbing system of the 2007–2008 dome-forming eruption of Kelut volcano, East
984   Java, Indonesia. *Contrib. Mineral. Petrol.* **166**, 275-308.

985 Kayzar, T.M., Cooper, K.M., Reagan, M.K. and Kent, A.J.R (2009). Gas transport model for
986   the magmatic system at Mount Pinatubo, Philippines: Insights from $(^{210}Pb)/(^{226}Ra)$. *J.*
987   *Volc. Geotherm. Res*. **181**, 124-140.

988 Komorowski J-C., Jenkins S., Baxter P.J., Picquout A., Lavigne F., Charbonnier S., Gertisser,
989   R., Preece K., Cholik N., Budi-Santoso A. and Surono (2013) Paroxysmal dome
990   explosion during the Merapi 2010 eruption: Processes and facies relationships of
991   associated high-energy pyroclastic density currents. *J. Volc. Geotherm. Res*. **261**, 260-
992   294.

993 Lambert G., Le Cloarec M.F., Ardouin B. and Le Roulley J.C. (1985) Volcanic emission of
994   radionuclides and magma dynamics. *Earth Planet. Sci. Lett.* **76**, 185–192.

995 Le Cloarec M-F and Gauthier P-J (2003). Merapi Volcano, Central Java, Indonesia: A case
996   study of radionuclide behavior in volcanic gases and its implications for magma
997   dynamics at andesitic volcanoes. J Geophys Res **108**, (B5) 2243

998 McDermott F. and Hawkesworth C. (1991) Th, Pb, and Sr isotope variations in young island
999   arc volcanics and oceanic sediments. Earth Planet Sci Lett, **104** 1-15.

1000 Nadeau O., Williams-Jones A.E., Stix J. (2013). Magmatic-hydrothermal evolution and
1001   devolatilization beneath Merapi volcano, Indonesia. *J Volc Geotherm Res* **261**, 50-68.

1002 Newhall C.G., Bronto S., Alloway B., Banks N.G., Bahar I., del Marmol M.A., Hadisantono
1003   R.D., Holcomb R.T., McGeehin J., Miksic J.N., Rubin M., Sayudi S.D., Sukhyar R.,
1004   Andreastuti S., Tilling R.I., Torley R., Trimble D. and Wirakusumah A.D. (2000)
1005   10,000 Years of explosive eruptions of Merapi Volcano, Central Java: archaeological
1006   and modern implications. *J. Volc. Geotherm. Res* **100**, 9-50.

1007   Nguyen, C.T., Gonnermann, H.M., Houghton, B.F. (2014). Explosive to effusive transition
1008   during the largest volcanic eruption of the 20th century (Novarupta 1912, Alaska).
1009   *Geology* **42** (8), 703-706.

1010   Pallister J.S., Schneider D.J., Griswold J.P., Keeler R.H., Burton W.C., Noyles C., Newhall
1011   C.G. and Ratdomopurbo A. (2013). Merapi 2010 eruption - chronology and extrusion
1012   rates monitored with satellite radar and used in eruption forecasting. *J. Volc. Geotherm.*
1013   *Res* **261**, 144-152.

1014   Peate D.W. and Hawkesworth C.J. (2005). U-series disequilibria: insights into mantle
1015   melting and the time scales of magma differentiation. *Rev. Geophys.* **43** RG1003, 1-
1016   43pp.

1017   Pin C. and Zalduegui J.F.S. (1997) Sequential separation of light rare-earth elements, thorium
1018   and uranium by miniaturized extraction chromatography: Application to isotopic
1019   analyses of silicate rocks. *Analytica Chimica Acta* **339**, 79-89.

1020   Plank T. and Langmuir C.H. (1998). The chemical composition of subducting sediment and
1021   its consequences for the crust and mantle. *Chem. Geol.* **145**, 325–394.

1022   Preece K.J. (2014). Transitions between effusive and explosive activity at Merapi volcano,
1023   Indonesia: a volcanological and petrological study of the 2006 and 2010 eruptions.
1024   *Ph.D. Thesis*. University of East Anglia, UK.

1025   Preece K., Barclay J., Gertisser R. and Herd R.A. (2013). Textural and micro-petrological
1026   variations in the eruptive products of the 2006 dome-forming eruption of Merapi
1027   volcano, Indonesia: implications for sub-surface processes. *J. Volc. Geotherm. Res* **261**,
1028   98-120.

1029   Preece K., Gertisser R., Barclay J., Berlo K., Herd R.A. and Edinburgh Ion Microprobe
1030   Facility (2014) Pre- and syn-eruptive degassing and crystallisation processes of the
1031   2010 and 2006 eruptions of Merapi volcano, Indonesia. *Contrib Mineral Petrol* **168**,
1032   1061.

1033   Preece K., Gertisser R., Barclay J., Charbonnier J., Komorowski J.-C. and Herd R.A. (2016)
1034   Transitions between explosive and effusive phases during the cataclysmic 2010
1035   eruption of Merapi volcano, Java, Indonesia. *Bull Volcanol* **78**, 54

1036   Ratdomopurbo A., Beauducel F., Subandriyo J., Agung Nandaka I.G.M., Newhall C.G.,
1037   Suharna Sayudi D.S., Suparwaka H. and Sunarta S (2013) Overview of the 2006
1038   eruption of Mt. Merapi. Journal of Volcanology and Geothermal Research 261: 97-97.

1039　Reagan, M., Tepley III, F.J., Gill, J.B., Wortel, M. and Hartman, B. (2005). Rapid time scales
1040　　　　of basalt to andesite differentiation at Anatahan volcano, Mariana Islands. *J. Volc.*
1041　　　　*Geotherm. Res* **146**, 171-183.

1042　Reagan M.K., Tepley III F.J., Gill J.B., Wortel M. and Garrison J. (2006). Timescales of
1043　　　　degassing and crystallization implied by ^{210}Po–^{210}Pb–^{226}Ra disequilibria for andesitic
1044　　　　lavas erupted from Arenal volcano. *J. Volc. Geotherm. Res* **157**, 135–146.

1045　Reagan, M., Turner S., Handley, H., Turner, M., Beier, C., Caulfield, J. and Peate, D. (2017).
1046　　　　^{210}Pb-^{226}Ra disequilibria in young gas-laden magmas. *Sci. Reports* 7:45186.

1047　Reagan M.K., Cooper K.M., Pallister J.S., Thornber C.R. and Wortel M. (2008). Timing of
1048　　　　Degassing and Plagioclase Growth in Lavas Erupted from Mount St. Helens, 2004–
1049　　　　2005, from ^{210}Po-^{210}Pb-^{226}Ra Disequilibria. A Volcano Rekindled: The Renewed
1050　　　　Eruption of Mount St. Helens, 2004–2006, Edited by David R. Sherrod, William E.
1051　　　　Scott, and Peter H. Stauffer *U.S. Geological Survey Professional Paper* **1750**, 847-
1052　　　　856.

1053　Reubi O., Sims K.W.W. and Bourdon B. (2014). ^{238}U–^{230}Th equilibrium in arc magmas and
1054　　　　implications for the timescales of mantle metasomatism. Earth Planet Sci Lett **391**, 146-
1055　　　　158.

1056　Rubin K.H. and Macdougall J. D. (1989) Submarine magma degassing and explosive
1057　　　　magmatism at Macdonald (Tamarii) seamount. *Nature* **341**, 50-52.

1058　Rubin K.H. (2001) Analysis of ^{232}Th/^{230}Th in volcanic rocks: A comparison of thermal
1059　　　　ionization mass spectrometry and other methodologies. *Chem Geol* **175**, 723-750.

1060　Sendjaja Y.A., Kimura J.-I. and Sunardi E. (2009). Across-arc geochemical variation of
1061　　　　Quaternary lavas in West Java, Indonesia: Mass-balance elucidation using arc basalt
1062　　　　simulator model. *Island Arc* **18**: 201-224.

1063　Sims K.W.W., Pichat S., Reagan M.K., Kyle P.R., Dulaiova H., Dunbar N.W., Prytulak J.,
1064　　　　Sawyer G., Layne G.D., Blichert-Toft J., Gauthier P.J., Charette M.A. and Elliott T.R.
1065　　　　(2013) On the time scales of magma genesis, melt evolution, crystal growth rates and
1066　　　　magma degassing in the Erebus volcano magmatic system using the ^{238}U, ^{235}U and
1067　　　　^{232}Th decay series. J Petrol **54**, 235-271.

1068　Sims K.W.W., Gill J., Dosseto A., Hoffmann D.L., Lundstrom C., Williams R., Ball L.,
1069　　　　Tollstrup D., Turner S., Prytulak J., Glessner J., Standish J. and Elliott T. (2008). An
1070　　　　inter-laboratory assessment of the Th isotopic composition of synthetic and rock
1071　　　　standards. *Geostandards Geoanalytical Res* **32**, 65-91.

1072 Staudigel H., Davies G.R., Hart S.R., Marchant K.M. and Smith B.M. (1995). Large scale
1073   isotopic Sr, Nd and O isotopic anatomy of altered oceanic crust: DSDP/ODP Sites
1074   417/418. *Earth Planet. Sci. Lett.* **130** 169-185.

1075 Surono, Jousset P., Pallister J., Boichu M., Buongiorno M.F., Budisantoso A., Costa F.,
1076   Andreastuti S., Prata F., Schneider D., Clarisse L., Humaida H., Sumarti S., Bignami
1077   C., Griswold J., Carn S., Oppenheimer C. and Lavigne F. (2012). The 2010 explosive
1078   eruption of Java's Merapi volcano - A '100-year' event. *J. Volc. Geotherm. Res.* **241-242**, 121-135.

1080 Troll V.R., Hilton D.R., Jolis E.M., Chadwick J.P., Blythe L.S., Deegan F.M., Schwarzkopf
1081   L.M. and Zimmer M. (2012) Crustal CO_2 liberation during the 2006 eruption and
1082   earthquake events at Merapi volcano, Indonesia. *Geophys Res Lett* **39**, L11302.

1083 Troll V.R., Deegan F.M., Jolis E.M., Harris C., Chadwick J.P., Gertisser R., Schwarzkopf
1084   L.M., Borisova A.Y., Bindeman I.N., Sumarti S. and Preece K. (2013) Magmatic
1085   differentiation processes at Merapi volcano: inclusion petrology and oxygen isotopes. *J. Volc. Geotherm. Res.* **261**: 38-49.

1087 Turner S. and Hawkesworth C. (1997). Constraints on flux rates and mantle dynamics
1088   beneath island arcs from Tonga–Kermadec lava geochemistry. *Nature* **389**, 568-573.

1089 Turner S., Evans P. and Hawkesworth C. (2001) Ultrafast source-to-surface movement of
1090   melt at island arcs from ^{226}Ra-^{230}Th Systematics. *Science* **292**, 1363-1366.

1091 Turner S, Bourdon B and Gill J (2003). Insights into Magma Genesis at Convergent Margins
1092   from U-series Isotopes. In: Bourdon, B., Henderson, G.M., Lundstrom, C.C., Turner,
1093   S.P. (Eds.), Uranium Series Geochemistry. *Reviews in Mineralogy and Geochemistry*,
1094   **52**. The Mineralogical Society of America, Washington, DC, pp. 255-315.

1095 Turner S., Black S. and Berlo K. (2004). ^{210}Pb–^{226}Ra and ^{228}Ra–^{232}Th systematics in young
1096   arc lavas: implications for magma degassing and ascent rates. Earth Planet Sci Lett **227**,
1097   1-16.

1098 Turner S.P., George R.M.M., Evans P.J., Hawkesworth C.J. and Zellmer G.F. (2000).
1099   Timescales of magma formation, ascent and storage beneath subduction zone
1100   volcanoes. *Philos. Trans. R. Soc. Lond.* **358**, 1443–1464.

1101 Turner S., Beier C. Niu Y. and Cook C. (2011).U-Th-Ra disequilibria and the extent of off‐
1102   axis volcanism across the East Pacific Rise at 9°30'N, 10°30'N, and 11°20'N,
1103   *Geochem. Geophys. Geosyst.* **12**, Q0AC12, doi:10.1029/2010GC003403.

1104   Van der Zwan F.M., Chadwick J.P. and Troll V.R. (2013) Textural history of recent basaltic-
1105   andesites and plutonic inclusions from Merapi volcano. *Contrib Mineral Petrol* **166**,
1106   43-63.

1107   Voight B., Constantine E.K., Siswowidjoyo S. and Torley R. (2000). Historical eruptions of
1108   Merapi volcano, Central Java, Indonesia, 1768-1998. *J. Volc. Geotherm. Res.* **100**: 69-
1109   138.

1110   Vukadinovic D. and Sutawidjaja I. (1995) Geology, mineralogy and magma evolution of
1111   Gunung Slamet Volcano, Java, Indonesia. *J Southeast Asian Earth Sci* **11**, 135-164.

1112   Waters C.L., Sims K.W.W., Klein E.M., White S.M., Reagan M.K. and Girard G. (2013) Sill
1113   to surface: Linking young off-axis volcanism with subsurface melt at the overlapping
1114   spreading center at 9º03'N East Pacific Rise. *Earth Planet. Sci. Lett.* **369-370**, 59-70.

1115   White W. M. and Patchett J. (1984) Hf-Nd-Sr isotopes and incompatible element abundances
1116   in island arcs: implications for magma origins and crustal-mantle evolution. *Earth
1117   Planet. Sci. Lett.* **67**, 167-185.

1118   Woodhead J.D., Hergt J.M., Davidson J.P. and Eggins S.M. (2001). Hafnium isotope
1119   evidence for 'conservative' element mobility during subduction processes. *Earth
1120   Planet. Sci. Lett.* **192**, 331–346.

1121   Zobin V.M., Arámbula, R., Bretón, M., Reyes, G., Plascencia, I., Navarro, C., Téllez, A.,
1122   Campos, A., González, M., León, Z., Martínez, A. and Ramírez, C. (2015). Dynamics
1123   of the January 2013–June 2014 explosive-effusive episode in the eruption of Volcán de
1124   Colima, México: insights from seismic and video monitoring. *Bull. Volcanol.* 77: 31.

Figure 1

Figure 2

Figure 3

Figure 3

Figure 4

Figure 5

Figure 6

2006

2010

C $(^{210}Po/^{210}Pb)$ → weeks to months

$^{210}Po_{gas}$

$(^{210}Po/^{210}Pb)$ → weeks to months

$^{222}Rn_{gas}$

B $(^{210}Pb/^{226}Ra)$ → ~2-4 years

$(^{210}Pb/^{226}Ra)$ → ~0-3 years

$^{226}Ra_{carb}$?
$^{238}U_{carb}$?

A $(^{226}Ra/^{230}Th)$ → 10^2-10^3 years

$(^{238}U/^{230}Th)$ → $<10^5$ years

$(^{226}Ra/^{230}Th)$ → 10^2-10^3 years

$(^{238}U/^{230}Th)$ → $<10^5$ years

$^{226}Ra_{fluid}$
$^{238}U_{fluid}$
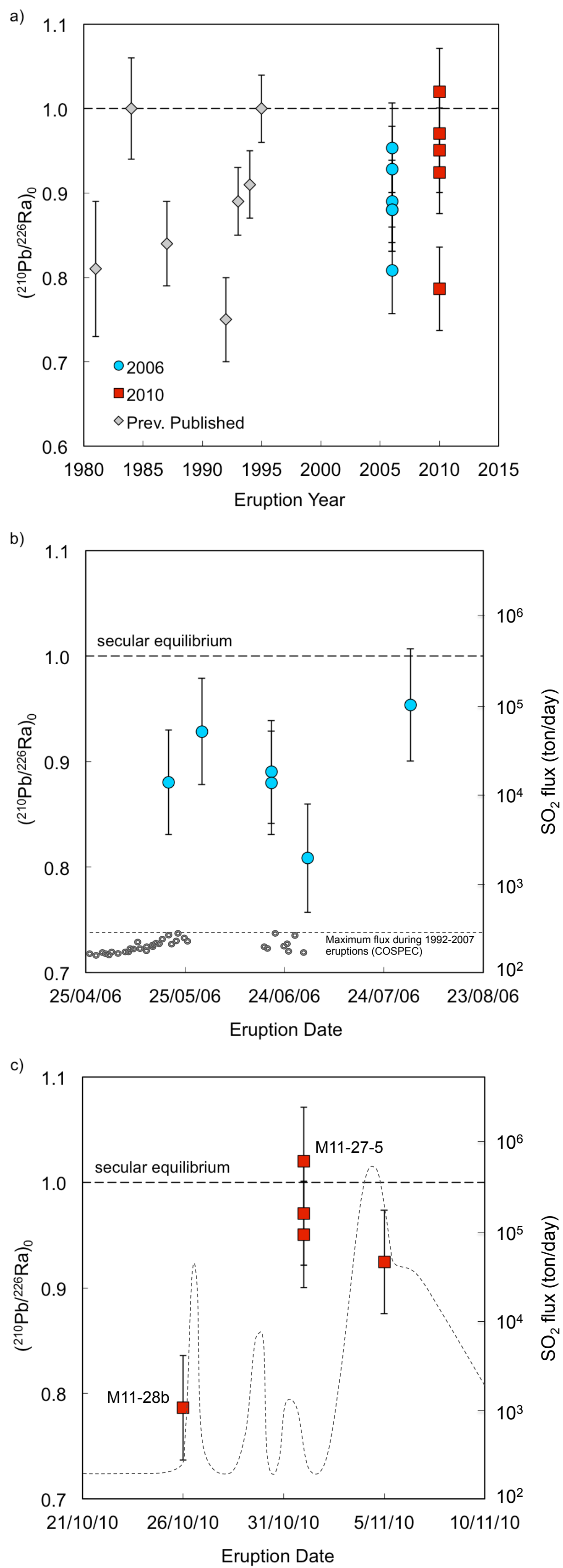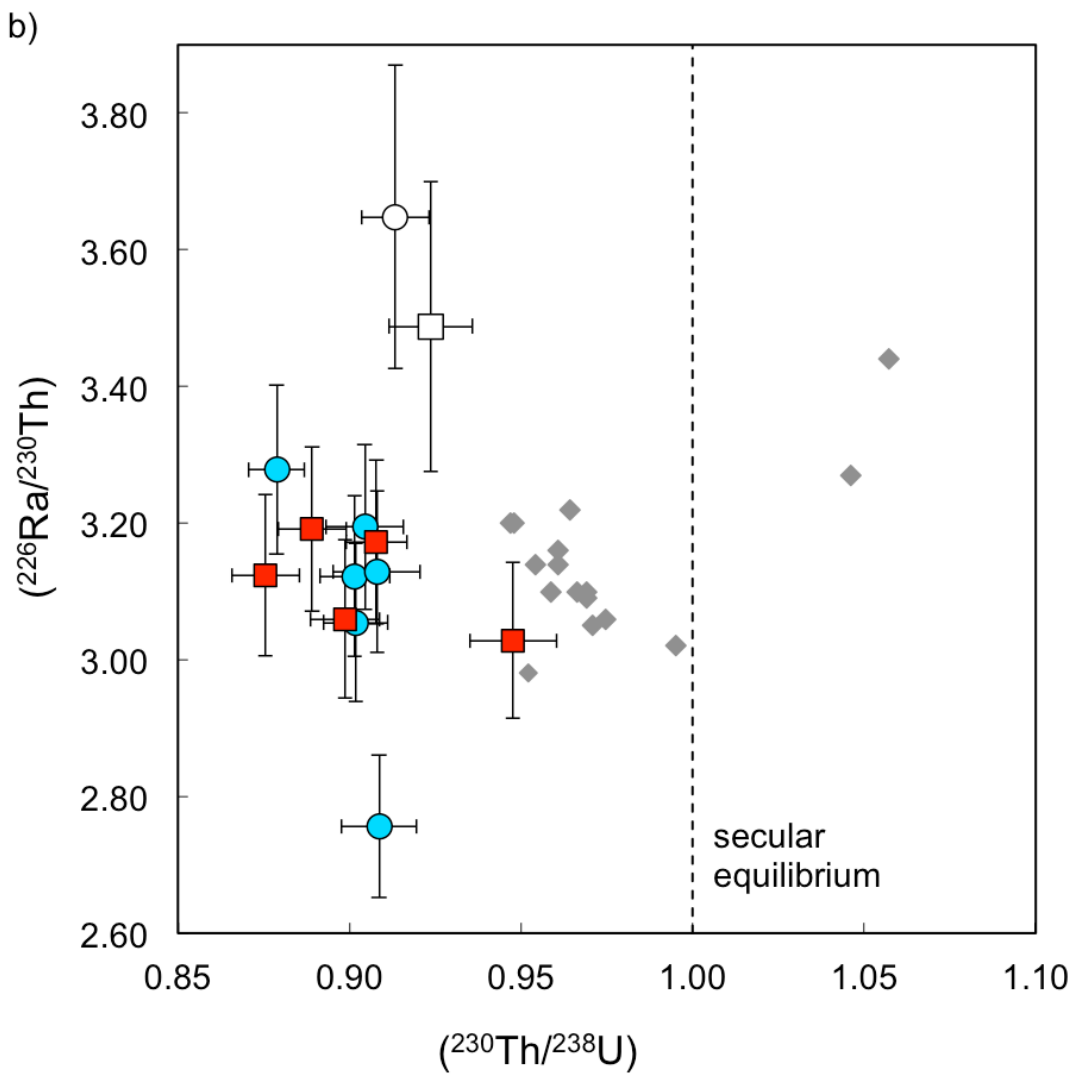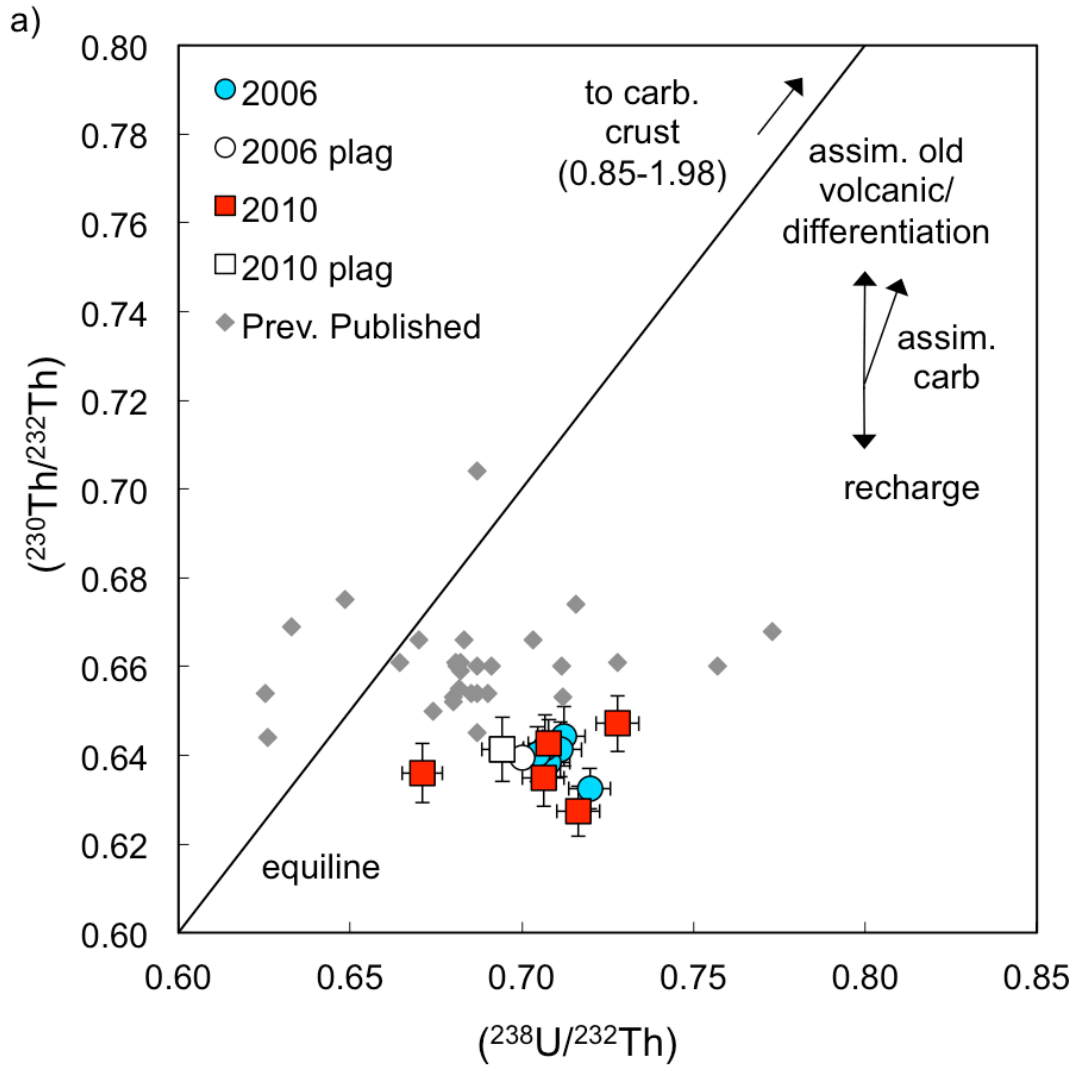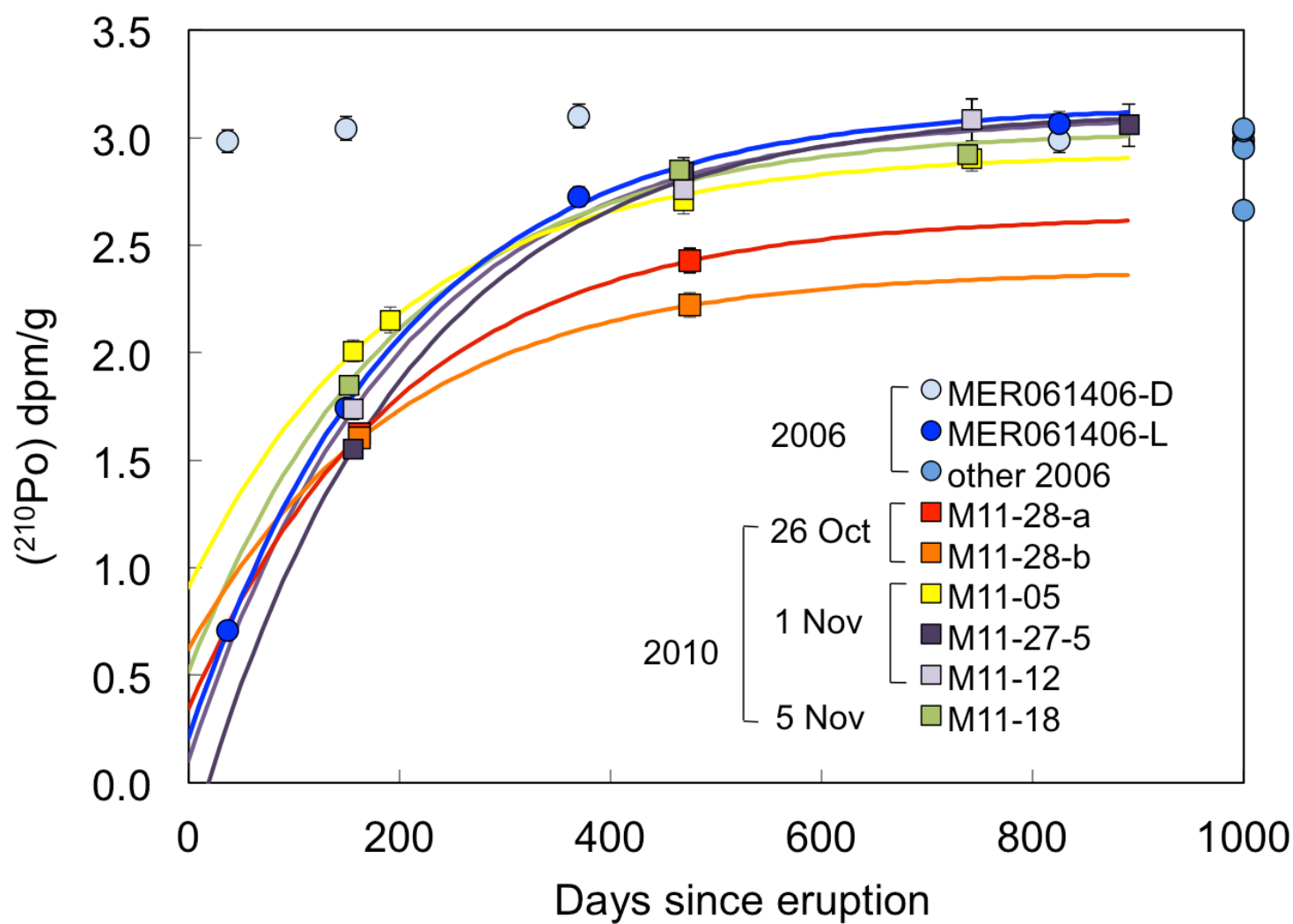
Table 1

Table 1. Uranium-series whole-rock and plagioclase separate data for the 2006 and 2010 Merapi volcanic rocks

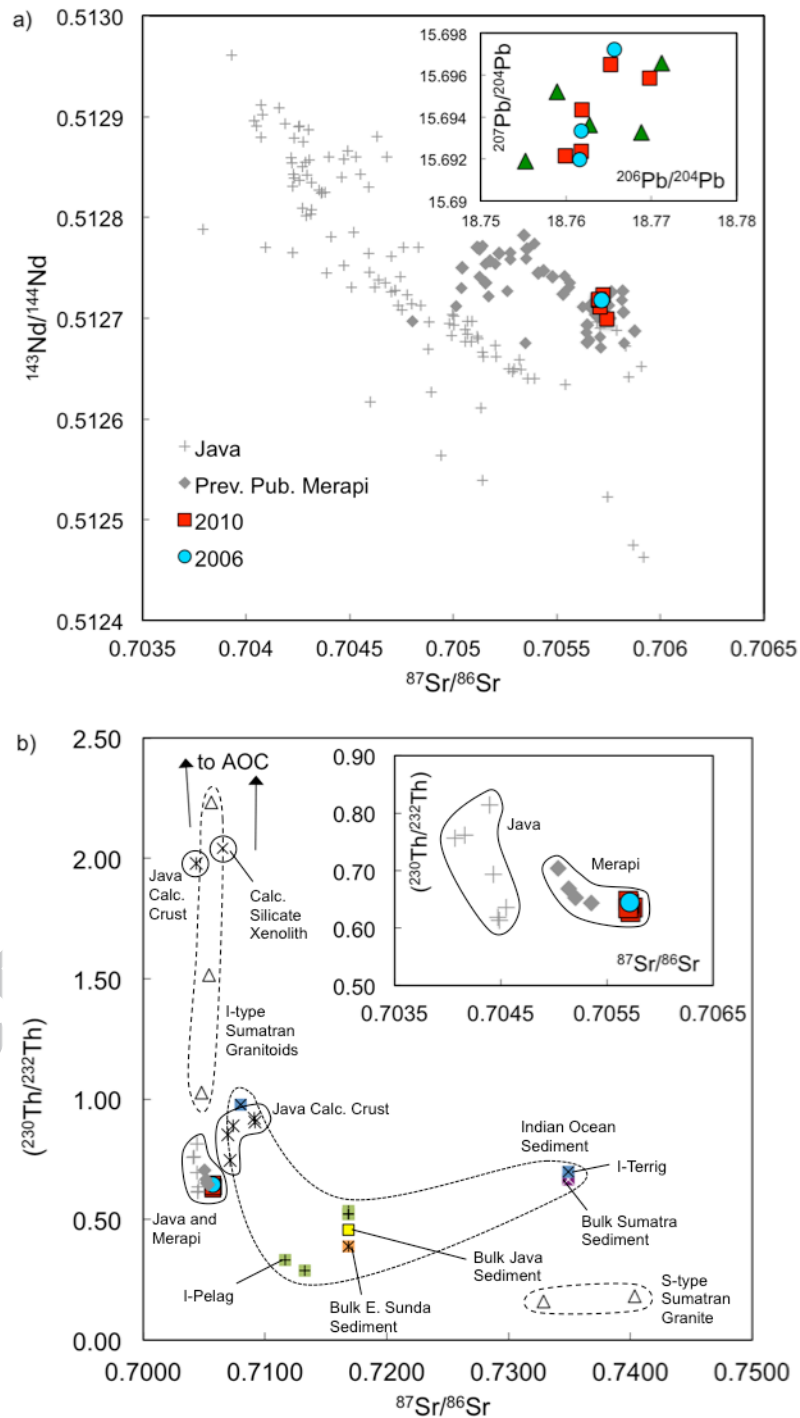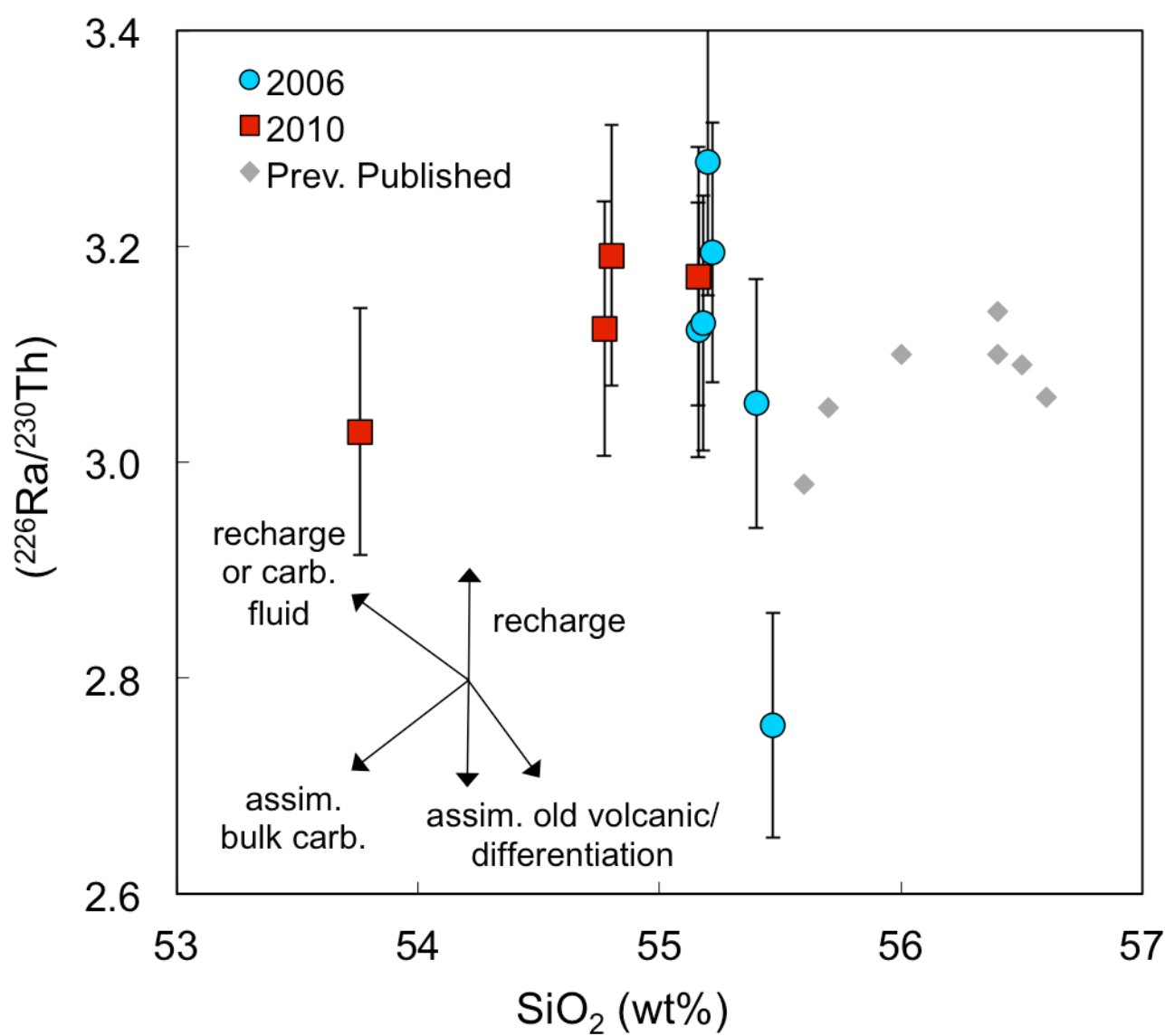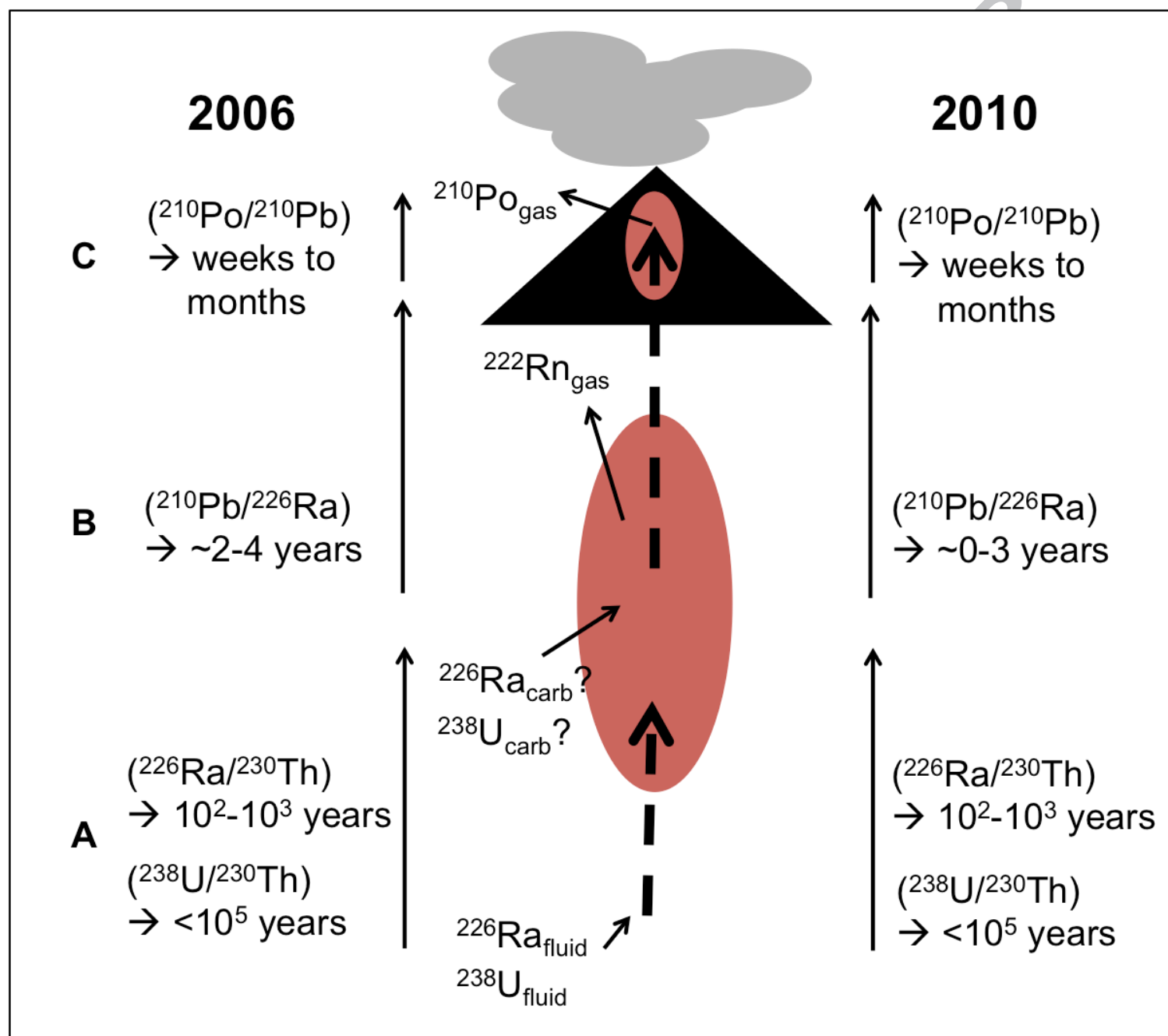| Sample Name	Sample Type	Stage	Eruption Age	SiO$_2$	[U]	±	[Th]	±	(^{234}U/^{238}U)	±	(^{238}U/^{232}Th)	±	(^{230}Th/^{232}Th)	±	(^{230}Th/^{238}U)	±
ME08-10	Kali Bebeng Scoria (KB-S)	I	20/05/2006[a]	55.18	1.55	0.04	6.67	0.08	1.003	0.005	0.702	0.006	0.642	0.007	0.914	0.013
M07-53	Lobe 1 - Scoria (L1-S)	II	30/05/2006[b]	55.22	1.50	0.03	6.39	0.08	1.004	0.005	0.712	0.006	0.644	0.007	0.904	0.011
M07-53P	Lobe 1 - Scoria Plagioclase (L1-S-Plag)	II	30/05/2006[b]	n.d.	0.35	0.01	1.51	0.02	1.003	0.005	0.700	0.006	0.640	0.006	0.913	0.010
M07-53P (*rpt*)	Lobe 1 - Scoria Plagioclase (L1-S-Plag)	II	30/05/2006[b]	n.d.	0.35	0.01	1.51	0.02	1.004	0.005	0.703	0.006	0.640	0.006	0.911	0.010
ME08-01	Lobe 4 - Scoria (L4-S)	III	20/06/2006[c]	55.16	1.59	0.04	6.78	0.08	1.002	0.005	0.711	0.006	0.641	0.006	0.901	0.010
ME08-04	Lobe 8 - Scoria (L8-S)	III	20/06/2006[c]	55.40	1.62	0.04	6.94	0.09	1.008	0.005	0.708	0.006	0.638	0.005	0.902	0.009
ME08-07	Lobe 10 - Scoria (L10-S)	III	01/07/2006[c]	55.20	1.49	0.03	6.23	0.08	1.002	0.005	0.720	0.006	0.633	0.005	0.879	0.008
ME08-14	Summit Dome Scoria (SD-S)	IV	01/08/2006[d]	55.47	1.64	0.04	7.06	0.09	1.004	0.005	0.705	0.006	0.640	0.006	0.909	0.011
M11-28b	Light Grey Dense Inclusion (LGD-Inc)	2	26/10/2010	n.d.	1.47	0.03	6.33	0.08	1.006	0.005	0.706	0.006	0.635	0.006	0.899	0.010
M11-05	Light Grey Dense Inclusion (LGD-Inc)	4	01/11/2010[e]	53.76	1.44	0.03	6.49	0.08	1.003	0.005	0.671	0.006	0.636	0.007	0.948	0.013
M11-05 (*rpt*)	Light Grey Dense Inclusion (LGD-Inc)	4	01/11/2010[e]	53.76	1.46	0.03	6.63	0.08	1.003	0.005	0.670	0.006	0.634	0.006	0.946	0.011
M11-12	Dome Dense (DD)	4	01/11/2010[e]	54.77	1.57	0.04	6.64	0.08	1.004	0.005	0.717	0.006	0.627	0.006	0.876	0.010
M11-27-5	Dome Dense (DD)	4	01/11/2010[e]	54.80	1.45	0.03	6.03	0.07	1.004	0.005	0.728	0.006	0.647	0.006	0.889	0.010
M11-01P	Dome Plagioclase (DD-Plag)	4	01/11/2010[e]	n.d.	0.24	0.01	1.03	0.01	1.004	0.005	0.694	0.006	0.641	0.007	0.924	0.012
M11-18	White Pumice (WP)	6	05/11/2010	55.16	1.53	0.03	6.54	0.08	1.002	0.005	0.708	0.006	0.643	0.005	0.908	0.009
TML	Std (Ra)						29.8	0.138					1.090		1.070	0.010
TML	Std (U-Th)				10.7	0.026	29.8	0.081	1.002	0.003	1.067	0.006	1.067	0.007	0.979	0.009
TML	Std (U-Th)				10.9	0.021	30.1	0.064	1.005	0.003	1.097	0.004	1.066	0.005	0.972	0.007
Average TML					10.8		29.9		1.003		1.094		1.068		0.975	
2 Std. Dev.					0.24		0.37		0.005		0.009		0.004		0.009	

Sample Name	Sample Type	Stage	Eruption Age	^{226}Ra (fg/g)	±	(^{226}Ra/^{230}Th)	±
ME08-10	Kali Bebeng Scoria (KB-S)	I	20/05/2006[a]	1501	19	3.13	0.12
M07-53	Lobe 1 - Scoria (L1-S)	II	30/05/2006[b]	1474	19	3.19	0.12
M07-53P	Lobe 1 - Scoria Plagioclase (L1-S-Plag)	II	30/05/2006[b]	395	23	3.65	0.22
M07-53P (*rpt*)	Lobe 1 - Scoria Plagioclase (L1-S-Plag)	II	30/05/2006[b]	379	22	3.49	0.21
ME08-01	Lobe 4 - Scoria (L4-S)	III	20/06/2006[c]	1522	19	3.12	0.12
ME08-04	Lobe 8 - Scoria (L8-S)	III	20/06/2006[c]	1517	19	3.05	0.12
ME08-07	Lobe 10 - Scoria (L10-S)	III	01/07/2006[c]	1449	18	3.28	0.12
ME08-14	Summit Dome Scoria (SD-S)	IV	01/08/2006[d]	1398	18	2.76	0.10
M11-28b	Light Grey Dense Inclusion (LGD-Inc)	2	26/10/2010	1378	17	3.06	0.12
M11-05	Light Grey Dense Inclusion (LGD-Inc)	4	01/11/2010[e]	1402	18	3.03	0.11
M11-05 (*rpt*)	Light Grey Dense Inclusion (LGD-Inc)	4	01/11/2010[e]	1390	18	2.95	0.11
M11-12	Dome Dense (DD)	4	01/11/2010[e]	1458	18	3.12	0.12
M11-27-5	Dome Dense (DD)	4	01/11/2010[e]	1396	18	3.19	0.12
M11-01P	Dome Plagioclase (DD-Plag)	4	01/11/2010[e]	258	15	3.49	0.21
M11-18	White Pumice (WP)	6	05/11/2010	1496	19	3.17	0.12
TML	Std (Ra)			3594	26	1.005	0.008

Sample types following Preece (2014) and Preece et al. (2016). SiO$_2$ (wt %) from Preece et al. (2013) and Preece (2014).

The 2006 eruption stage is taken from Charbonnier and Gertisser (2008) as detailed in Preece et al. (2013). The 2010 eruption stage is taken from Komorowski et al. (2013) as detailed in Preece et al. (2016).

[a]ME08-10 extruded between 1 May and 1 June 2006 and was emplaced 11 May to 1 June.

[b]M07-53 emplaced in BAFs on 14 June, but extruded between 1st May to 14th June. Microlite textures and lack of amphibole reaction rims in these samples extruded not long before collapse (Preece et al. 2016).

[c]Stage III 2006 samples: extruded post-14 June. Exact date of collapse not know, extrusion between 15 June and early July 2006.

[d]Stage IV 2006 sample: extrusion 15 June - Oct 2006, so an intermediate date in August is assumed for plotting purposes (sample collected in 2008 from the uncollapsed part of the 2006 summit dome).

[e]Samples extruded during Stage 3, between 29 October and 4 November 2010 and emplaced in BAFs and surges on 5 Nov (Stage 4). An intermediate eruption date of 1 November 2010 was used for plotting.

rpt = sample repeat including digestion. n.d. = not determined. Errors on TML are 2SE (measurement precision). Errors given on samples represent 2σ precisions based on TML and sample reproducabilities.

Table 2

Table 2. Measured and initial ^{210}Po and ^{210}Pb activities and (^{210}Po/^{210}Pb) and (^{210}Pb/^{226}Ra) in Merapi volcanic rock samples

Sample Name	Sample Type	Eruption/Extrusion Date	Analysis Day	$(^{210}Po)_m$ dpm/g	± 2S	$(^{210}Po)_i$	± 2S	$(^{210}Pb)_i$	± 2S	$(^{210}Po/^{210}Pb)_i$	^{210}Po Degassed (%)	$(^{210}Pb/^{226}Ra)_0$	± 2S	Years Degassing
MER 95		1995	>700	3.10	0.06			3.05	0.16					
ME08-10	KB-S	20/05/2006	>700	2.96	0.07			2.90	0.09			0.88	0.05	4
ME08-10 (rpt)	KB-S	20/05/2006	>700	2.99	0.07									
M07-53	L1-S	30/05/2006	>700	3.04	0.07			3.01	0.09			0.93	0.06	2
ME08-01	L4-S	20/06/2006	>700	3.03	0.07			2.98	0.09			0.89	0.05	4
ME08-01 (rpt)	L4-S	20/06/2006	>700	3.06	0.07									
ME08-04	L8-S	20/06/2006	>700	2.99	0.07			2.93	0.09			0.88	0.05	4
ME08-04 (rpt)	L8-S	20/06/2006	>700	3.02	0.07									
ME08-07	L10-S	01/07/2006	>700	2.66	0.07			2.57	0.09			0.81	0.06	7
ME08-14	SD-S	01/08/2006	>700	2.95	0.07			2.93	0.09			0.95	0.06	2
MER061406-L	GR-LGS	14/06/2006	37	0.71	0.02	0.21	0.2	3.15	0.10	0.07	93			
			149	1.74	0.04									
			370	2.73	0.05									
			825	3.06	0.06									
MER061406-LL8	leachate	14/06/2006	37	3.81	0.42									
MER061406-D	GR-DGS	14/06/2006	37	2.98	0.05	2.95	0.2	3.12	0.10	0.95				
			149	3.04	0.05									
			370	3.10	0.06									
MER061406-DL8	leachate	14/06/2006	37	2.84	0.32									
M11-28a	S2S	26/10/2010	162	1.62	0.04	0.34	0.20	2.64	0.15	0.13	87			
			475	2.43	0.06									
M11-28b	LGD-Inc	26/10/2010	162	1.60	0.04	0.62	0.20	2.38	0.16	0.26	74	0.79	0.10	8
			475	2.22	0.06									
M11-05	LGD-Inc	1/11/2010	156	2.01	0.05	0.91	0.10	2.93	0.11	0.31	69	0.95	0.07	2
			191	2.15	0.06									
			469	2.71	0.06									
			742	2.90	0.06									
M11-12	DD	1/11/2010	156	1.74	0.05	0.10	0.20	3.11	0.11	0.03	97	0.97	0.07	1
			469	2.76	0.06									
			742	3.08	0.10									
M11-27-5	DD	1/11/2010	156	1.55	0.04	-0.30	0.20	3.13	0.12	-0.10	100	1.02	0.07	0
			469	2.84	0.07									
			891	3.06	0.10									
M11-01P	DD-Plag	1/11/2010	>700	1.12	0.08			1.12	0.10			1.97	0.42	
M11-18	WP	5/11/2010	152	1.85	0.05	0.52	0.20	3.04	0.11	0.17	83	0.92	0.07	3
			465	2.85	0.06									
			738	2.92	0.06									
BCR-2	Rock Standard			1.27	0.04									
BCR-2	Rock Standard			1.24	0.04									

Analysis Day is days after the eruption date. For details on sample eruption date see Table 1. Radium activity is taken from Table 1.

Sample types are given in Table 1. S2S = Pre Nov 5 Scoria; GR-LGS = Gendol River, Light Grey Scoria; GR-DGS = Gendol River, Dark Grey Scoria.

MER061406-D is not a juvenile clast of the 2006 eruption (see text).

MER061406-L was taken from a PDC deposited on 14 June, the exact extrusion age is unknown.

Most 2006 samples were analysed 5-6 years after eruption, which is significantly greater than five times the half-life of ^{210}Po (138.4 days), therefore, (^{210}Pb) was considered equal to measured (^{210}Po) and analysis day is listed as >700 days.

For samples analysed soon after eruption, the initial ^{210}Pb activities, (^{210}Pb)$_i$, representing ^{210}Pb activity at the time of eruption, were calculated using a Matlab code (see text).

The initial ^{210}Pb activities for M11-28a and M11-28b are likely carry greater uncertainty than that shown as they are based on only 2 (^{210}Po) measurements.

The years of magmatic degassing (prior to eruption) is calculated using (^{210}Pb/^{226}Ra)$_0$ and assuming: 1) the simplest model of efficient (complete) removal of ^{222}Rn, 2) that the influence of carbonate assimilation is similar for all samples and, 3) a system closed to magmatic recharge (Equation 11 of Gauthier and Condomines, 1999).

The percentage of ^{210}Po degassed on eruption is calculated using the degassing efficiency factor equation given in Gill et al., 1985.

Table 3

ACCEPTED MANUSCRIPT

Table 3. Sr, Nd and Pb isotopic data of the 2006 and 2010 Merapi volcanic rocks

Sample	$^{87}Sr/^{86}Sr$	2SE	$^{143}Nd/^{144}Nd$	2SE	$^{206}Pb/^{204}Pb$	$^{207}Pb/^{204}Pb$	$^{208}Pb/^{204}Pb$
M07-53	0.705714	0.000007	0.512718	0.000006	18.762	15.693	39.147
ME08-07					18.766	15.697	39.157
ME08-14					18.762	15.692	39.143
M11-05	0.705742	0.000007	0.512699	0.000008	18.770	15.696	39.162
M11-12	0.705722	0.000006	0.512723	0.000006	18.762	15.694	39.147
M11-18	0.705709	0.000027	0.512711	0.000007	18.762	15.692	39.125
M11-27-5	0.705701	0.000012	0.512718	0.000007	18.760	15.692	39.137
M11-28b	0.705702	0.000009	0.512719	0.000005	18.765	15.697	39.153
SRM 987	0.710214	0.000008					
JMC Nd			0.511116	0.000008			

Pb isotope data are from Handley et al. (2014).